AD NUMBER
AD617155
CLASSIFICATION CHANGES
TO: **UNCLASSIFIED**
FROM: **CONFIDENTIAL**
LIMITATION CHANGES
TO: **Approved for public release; distribution is unlimited.**
FROM: **Distribution authorized to U.S. Gov't. agencies only; Test and Evaluation; FEB 1958. Other requests shall be referred to Armed Forces Special Weapons Project, Albuquerque, NM. Formerly Restricted Data.**
AUTHORITY
28 Jun 1961, per document marking; DASA per document marking

AD NUMBER
AD617155
CLASSIFICATION CHANGES
TO: **CONFIDENTIAL**
FROM: **SECRET**
AUTHORITY
25 May 1960, per document marking

WT-1110

This document consists of 70 pages

No. 125 of 225 copies, Series A

Operation TEAPOT

NEVADA TEST SITE

February – May 1955

Project 1.11

SPECIAL MEASUREMENTS OF DYNAMIC PRESSURE VERSUS TIME AND DISTANCE

Issuance Date: February 28, 1958

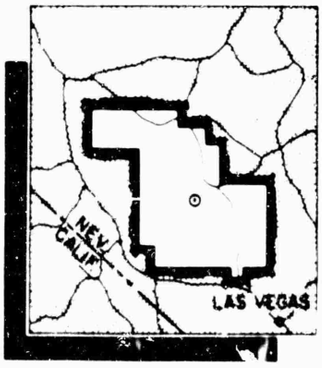

HEADQUARTERS FIELD COMMAND, ARMED FORCES SPECIAL WEAPONS PROJECT
SANDIA BASE, ALBUQUERQUE, NEW MEXICO

WT—1110

OPERATION TEAPOT—PROJECT 1.11

Report to the Test Director

SPECIAL MEASUREMENTS OF DYNAMIC PRESSURE VERSUS TIME AND DISTANCE

J. R. Banister
F. H. Shelton

Sandia Corporation
Albuquerque, New Mexico

SUMMARY OF SHOT DATA, OPERATION TEAPOT

Shot	Code Name	Date	Time*	Area	Type	Latitude and Longitude of Zero Point
1	Wasp	18 February	1200	T-7-4†	762-ft Air	37° 05' 11.6886" 116° 01' 18.7366"
2	Moth	22 February	0545	T-3	300-ft Tower	37° 03' 52.3854" 116° 01' 15.6967"
3	Tesla	1 March	0530	T-9b	300-ft Tower	37° 07' 31.5737" 116° 03' 51.0077"
4	Turk	7 March	0520	T-2	500-ft Tower	37° 06' 18.4944" 116° 07' 03.3279"
5	Hornet	12 March	0520	T-3a	300-ft Tower	37° 02' 25.4943" 116° 01' 31.2874"
6	Bee	22 March	0505	T-7-1a	500-ft Tower	37° 05' 41.3680" 116° 01' 25.5474"
7	ESS	23 March	1230	T-10a	67-ft Underground	37° 10' 04.1283" 116° 02' 37.7010"
8	Apple	29 March	0455	T-4	500-ft Tower	37° 05' 43.0200" 116° 06' 00.0046"
9	Wasp'	29 March	1000	T-7-4‡	740-ft Air	37° 05' 11.6886" 116° 01' 13.7366"
10	HA	6 April	1000	T-5§	36,620-ft MSL Air	37° 01' 43.3642" 116° 03' 25.2824"
11	Post	9 April	0430	T-9c	300-ft Tower	37° 07' 10.6965" 116° 02' 03.5960"
12	MET	15 April	1115	FF	400-ft Tower	36° 47' 52.6587" 115° 55' 44.1096"
13	Apple 2	5 May	0510	T-1	500-ft Tower	36° 03' 11.1005" 116° 06' 00.4937"
14	Zucchini	15 May	0500	T-7-1a	500-ft Tower	37° 05' 41.3680" 116° 01' 25.5474"

* Approximate local time, PST prior to 24 April, PDT after 24 April.
† Actual zero point 36 feet north, 426 feet west of T-7-4.
‡ Actual zero point 94 feet north, 62 feet west of T-7-4.
§ Actual zero point 36 feet south, 397 feet west of T-5.

ABSTRACT

Pitch and yaw of shock afterflow as a function of time, dynamic pressure parameters, and the contributions of air and dust to dynamic pressure were measured over desert, asphalt, and water surfaces during Shot 12.

Little or no yaw of flow was detected, but pitch of flow was found to be considerable over all three surfaces to 2,500 feet from ground zero. Over desert and asphalt, pitch-time records displayed a consistent pattern of initial upward flow followed by horizontal flow, or at 2,500-foot stations, downward flow. Pitch-time records over water are erratic and little understood.

Air dynamic pressures at 3-foot elevations, 2,000 and 2,500 feet from ground zero, were highest over desert and higher over asphalt than water. Considerable dust loading occurred on the desert where dust dynamic pressure exceeded that of air. Particle loading was present over asphalt, but the extent was not determined. No tangible evidence of water loading was found.

Results suggest that high air dynamic pressures over desert and asphalt arise from air velocities higher than would be expected from the Rankine Hugoniot relations and measured overpressures. Some speculations are made about possible causes of these high velocities.

FOREWORD

This report presents the final results of one of the 56 projects comprising the Military Effects Program of Operation Teapot, which included 14 test detonations at the Nevada Test Site in 1955.

For overall Teapot military-effects information, the reader is referred to "Summary Report of the Technical Director, Military Effects Program," WT-1153, which includes the following: (1) a description of each detonation including yield, zero-point environment, type of device, ambient atmospheric conditions, etc.; (2) a discussion of project results; (3) a summary of the objectives and results of each project; and (4) a listing of project reports for the Military Effects Program.

CONTENTS

ABSTRACT 5

FOREWORD 6

CHAPTER 1 INTRODUCTION 11
1.1 Objective 11
1.2 Background and Theory 11
1.2.1 Wind Direction 11
1.2.2 Dynamic Pressure 12

CHAPTER 2 INSTRUMENTATION 14
2.1 Wind Direction Gage 14
2.2 Snob and Greg Gages 14
2.3 Force Plate 15
2.4 Centripetal Density Gage 18
2.5 Particle-Velocity Gage 19
2.6 Medium-Density Gage 19
2.7 Value of Instrumentation 19

CHAPTER 3 EXPERIMENTAL PROCEDURE 22
3.1 Instrumentation Layout 22
3.2 Recording System 25

CHAPTER 4 RESULTS AND DISCUSSION 26
4.1 Data Reduction and Reading Techniques 26
4.2 Wind Direction Measurements 26
4.2.1 Pitch 26
4.2.2 Yaw 35
4.3 Other Measurements 37
4.3.1 Snob and Greg (Air and Dust Dynamic Pressures) 37
4.3.2 Force Plate 42
4.3.3 Centripetal Density (Air Density) 44
4.3.4 Particl. Velocity 50
4.3.5 Medium Density 50
4.3.6 Overpressure 53
4.3.7 Derived Quantities and Cross Checks 53
4.3.8 Comments on Errors 56
4.3.9 Shot 4 Results 56

CHAPTER 5 CONCLUSIONS AND RECOMMENDATIONS 57
5.1 Conclusions 57
5.1.1 Wind Direction Measurements 57
5.1.2 Other Measurements 57
5.1.3 General Conclusions 58
5.2 Recommendations 59

APPENDIX A THEORY OF THE SNOB AND GREG DUST RESPONSE 60

APPENDIX B THEORETICAL TREATMENT OF THE MEDIUM-DENSITY CAPACITY GAGE 63

APPENDIX C CORRECTION OF DYNAMIC PRESSURE FOR SPHERICAL DIVERGENCE 65

REFERENCES 68

TABLES

2.1 Basic Equalities and Cross Checks on Instrumentation 20
4.1 Initial Pitch Behavior, Shot 12 27
4.2 Pitot-Static Tube Dynamic Pressure Results, Shot 12..... 40
4.3 Shob Results, Shot 12 40
4.4 Greg Results, Shot 12 40
4.5 Force Plate Results, Shot 12..... 54
4.6 Centripetal Density Gage Results, Shot 12 54
4.7 Overpressure Measurements, Shot 12..... 54
4.8 Ambient Conditions for Shot 12 Surface 55
4.9 Shot 4 Results 55
C.1 Spherical Divergence Calculations 66

FIGURES

2.1 Calibration of Wind Direction Gage Used in the Pitch Sense (Shot 12) 16
2.2 Schematic Diagram of Wind Direction Gage 16
2.3 Schematic Diagram of Snob Gage 17
2.4 Schematic Diagram of Greg Gage Probe 17
3.1a Wind-Direction Gage Measuring Pitch at 1350 Feet on Shot 4 (Preshot) 23
3.1b Wind-Direction Gage Measuring Pitch at 1350 Feet on Shot 4 (Postshot) 23
3.2a Towers with Special Dynamic Pressure Instruments 24
3.2b Foreground Tower with "Baffleless" Centripetal Density Gage, Force Plate, Particle-Velocity Gage, and Wind-Direction Gage 24
3.2c Background Tower with Snob and Greg Gages, and an Unofficial Dust Sampler 25
4.1 Pitch-Time Records, Desert 29
4.2 Pitch-Time Records, Asphalt 31
4.3 Pitch-Time Records, Water 34
4.4 Maximum Initial Pitch versus Ground Distance (Desert) 36
4.5 Maximum Initial Pitch versus Ground Distance (Asphalt)..... 36
4.6 Duration of Initial Upward Flow Period as a Function of Ground Distance (Desert and Asphalt) 37
4.7 Pitch-Time History for Various Levels at 2,500 Feet (Desert) 38
4.8 Pitch-Time History for Various Levels at 2,500 Feet (Asphalt) 38
4.9 Gage Records, 2,000 Feet, Desert 41

4.10 Gage Records, 2,500 Feet, Desert 43
4.11 Gage Records, 2,000 Feet, Asphalt 44
4.12 Gage Records, 2,500 Feet, Asphalt 45
4.13 Gage Records, 2,000 Feet, Water 46
4.14 Gage Records, 2,500 Feet, Water 47
4.15 Various Measured and Derived Parameter-Time Records for 2,000 Feet (Desert) 48
4.16 Various Measured and Derived Paramter-Time Records for 2,500 Feet (Asphalt) 49
4.17 Various Measured and Derived Parameter-Time Records for 2,500 Feet (Asphalt) 50
4.18 Various Measured and Derived Parameter-Time Records for 2,000 Feet (Water) 51
4.19 Various Measured and Derived Parameter-Time Records for 2,500 Feet (Water) 52

Chapter 1
INTRODUCTION

1.1 OBJECTIVE

During Operation Upshot-Knothole, dynamic pressures measured in the precursor regions were almost ten times higher than calculated values, (from Rankine Hugoniot relations and measured overpressure) causing severe damage to drag-sensitive targets (Reference 1) and indicating that a drastic unknown mechanism was at work in the precursor afterflow. To explore this further, Operation Teapot Project 1.11 made special measurements versus time and distance over three surfaces: desert, asphalt, and water. The desert surface was intended to produce a dusty precursor, the asphalt a "clean" precursor, and the water surface an "ideal" blast wave (Reference 2). The three blast lines were instrumented to measure afterflow direction, air and dust contributions to and effect of obstacle size on dynamic pressure, and density and velocity of air and suspended dust. High dynamic pressure might then be explained, at least to the extent of knowing which factor or factors caused enhancement.

1.2 BACKGROUND AND THEORY

1.2.1 Wind Direction. Prior to this study, no measurements of vertical flow had been made within the precursor; however, photographs and the behavior of targets indicated that considerable pitch existed; precursor shocks were not perpendicular to the ground, and bridges, for example, appeared to be blown up from rather than off their supports (Reference 3).

One expects the flow behind a front advancing into still air to be normal to the front. The observed inclination of the precursor shock therefore implies that the flow is initially upward and only later settles down to horizontal flow. Near the ground the flow must always be horizontal; this means that the front must curve so as to be normal to the surface at its lower end.

Direct measurements of pitch, the vertical angle of flow, were indicated. They would give information about the precursor afterflow; any such data might reveal more about this little-understood phenomenon. They were also needed for correction of pitch-sensitive instruments and for determination of the direction of the shock-induced drag forces.

No precursor was expected over the water line; since the pitch-measuring stations were to be in the Mach stem, little or no pitch was expected. Nevertheless, pitch-time records were taken as a check on

instrumentation and to determine departures from "ideal" flow. Some measurements of yaw were also made to check cross-feed from the adjacent desert to the water line.

1.2.2 Dynamic Pressure. Air dynamic pressure (q_a) is defined by

$$q_a = 1/2\ \rho_a u_a^2 \qquad (1.1)$$

where ρ_a is air density and u_a is air velocity. For peak air dynamic pressures immediately behind a shock front or behind plane waves having a slow rise with an unchanging pressure profile, Equation 1.1 may be specialized by using values of ρ_a and u_a based on the Rankine Hugoniot relation. This result is

$$q_a = 2.5\ \frac{(\Delta P)^2}{7\ P_o + \Delta P} \quad , \qquad (1.2)$$

where P_o is ambient pressure and ΔP is overpressure. Equation 1.2 is valid up to shock strengths of 8; beyond this value, changes of the specific heat ratio (γ) began to be felt. It is, of course, physically impossible to obtain a slow rising plane wave of unchanging pressure profile equivalent to such a shock strength.

Equations 1.1 and 1.2 are somewhat idealized because air, a compressible fluid, does not register a difference between head-on and side-on pressure equal to $1/2\ \rho_a u_a^2$ but rather what we shall term observed dynamic pressure (q_{ac}). However, this observed quantity may easily be correlated with ideal by use of the relation

$$q_{ac} = q_a\ (1 + 0.25\ M^2 + 0.025\ M^4 + \ldots) \quad , \qquad (1.3)$$

where M is Mach number of free flow. Mathematically, this expression is valid for Mach numbers up to 2.22 for isentropic flow. Physically, a bow shock develops when the free flow Mach exceeds one and flow across it is accompanied by an entropy gain. This entropy gain is slight for Mach numbers less than 1.25; for that Mach number the error incurred in computing q_{ac} using Equation 1.3 amounts to two percent. If only the first two terms of Equation 1.3 are used the error is again about two percent while the error is of opposite sign.

Dynamic pressures behind the precursor blast waves of Upshot-Knothole (Reference 5) were not merely higher than Equation 1.2 and the observed overpressures would indicate, but they were about twice as high as would be expected over an ideal surface. This ideal surface, of course, has higher overpressures at the same ground distance than does a surface over which a precursor forms.

Four explanations of the anomaly have been offered:

1. It was caused by the Bernoulli effect and that in general the sum of dynamic pressure and overpressure is about the same for a precursor

wave as it is for an ideal at equal distances.[1] This was an intriguing concept, but it lacked intellectual satisfaction, i.e., one still wanted the effect "explained."

2. A pattern existed in the precursor afterflow which led to higher flow velocities than would be expected from Equation 1.2. The pattern was pictured as a quasi-steady circulation about a bubble formed in the heated air layer responsible for the precursor formation (Reference 4).

3. High dynamic pressures were caused by suspended dust carried along in the precursor afterflow. This was suggested by the fact dynamic pressure increased markedly when the dust cloud impinged on the gages. Furthermore, shock-tube experiments indicated that the gages used were sensitive to suspended dust. For small obstacles this increase in dynamic pressure is the free-stream momentum flux of suspended dust, thus

$$q_d = \rho_d u_d^2 \tag{1.4}$$

where q_d is the dynamic pressure caused by dust, ρ_d, the density of suspended dust, and u_d, the dust velocity (Reference 5).[2]

4. Pressure waves with slow rise times have dynamic pressures that are unrelated to extensions of Equation 1.2, that is, peak values of overpressure in a spherical or cylindrical shock wave with a slow rise time are not even approximate criteria for determining peak values of dynamic pressure (Reference 6).

---

[1] This concept may be oral only; at least the authors are not aware of a reference. However, the concept is widely known and may have been originated at a working conference on precursor phenomena at Headquarters, AFSWP prior to the Fourth Meeting of the AFSWP Height-of-Burst Panel on February 10, 1954.

[2] See Appendix A for further discussion of the dynamics of air dust mixtures.

Chapter 2
INSTRUMENTATION

Table 2.1 gives a list of gages, types of measurement obtained and available cross-checks. Some instruments were developed especially for Operation Teapot.

2.1 WIND DIRECTION GAGE[1]

This gage was used to obtain both pitch- and yaw-time records. Pitch is a deviation of flow-direction from parallel to the surface, upward flow being positive. Yaw is horizontal deviation of flow from a line joining the gage to ground zero, a clockwise deviation looking down on ground zero being considered positive.

The sensing element of the gage is a small vane soldered to a sturdy shaft (Figure 2.1). Several types of vanes are used to cover different dynamic pressure ranges; larger vanes are needed for lower dynamic pressures. In the presence of flow, the vane orients itself to minimize drag acting on it (zero torque). Reorientation time is about 3 to 7 msec, varying with the vane used, deflection required, and the dynamic pressure level. Rotation of the vane is transmitted by the shaft on which it is mounted to the moving contact arm of a small potentiometer,[2] providing a signal that is correlated with wind direction (Figure 2.2).

2.2 SNOB AND GREG GAGES (REFERENCE 7)

In clean air, snob (a pitot-static arrangement, Figure 2.3) obtains dynamic pressure and side-on pressure-time records, and greg (Figure 2.4) obtains head-on pressure-time records. Snob, however, has little response to the momentum flux of dust, while greg reacts fully to the same condition by showing an increased dynamic pressure which represents free-stream momentum flux of dust ($\rho_d u_d^2$),[3] where ρ_d is suspended dust density and u_d is dust velocity.

The small response of snob to dust results from the use of a special head-on pressure probe which has a small diameter and a streamlined tip.

---

[1] Developed by J. W. Wistor, of Sandia Corporation. A gage of similar principle but of lighter construction was unsuccessfully employed on Operation Tumbler-Snapper.

[2] The Microtorque, manufactured by Gianinni; it is linearly sensitive to rotations of half a degree.

[3] See Section 1.2 and Appendix A for theory of dynamic behavior of a dust-air mixture.

The head-on pressure is transmitted from a point close to the probe tip to the forward pressure transducer by a set of small pressure lines. The probe is also equipped with a long cylindrical cavity in which dust is decelerated and captured. Dust momentum flux is registered by the instrument only to the extent that dust loses its momentum before it reaches the head-on pressure-sensing region. The forward probe of snob has a considerable volume which fills through a small orifice, giving the gage a rise time of over 3 msec; fill volume is reduced somewhat by use of a flush diaphragm-type transducer. By situating eight inlet ports in the side-on sensing region which feed to a rear pressure transducer and to the back of the forward transducer, snob becomes a side-on and dynamic-pressure sensing gage.

The greg gage is much simpler (partly because it is solely a head-on pressure gage) and consists of a flush diaphragm pressure transducer protected by one or more layers of silicon rubber and mounted in a conventionally shaped probe, Figure 2.4.

Neither the snob nor the greg gage is significantly inclination-angle sensitive.

For dust particles of ordinary density, mean diameters in excess of 10 microns, and with velocities expected under field conditions, both instruments perform nearly perfectly. At Frenchman Flat, however, most of the dust particles have diameters below 10 microns, resulting in less satisfactory operation of the two instruments.[1] Calculations and blow-down tube tests indicate that for this small dust size, snob responds to 15 percent and greg responds to 90 percent of dust momentum flux. A further check of the response of the instruments is planned, using an improved blow-down tube arrangement.

Pressure transducers used in both instruments were manufactured by Ultradyne Engineering (Albuquerque, New Mexico) and are similar to a type previously manufactured and used by Sandia Corporation (Reference 8), except that one-half of the transducer was used to provide a flush diaphragm. A matching pressure-insensitive dummy was used to obtain a bridge balance. This arrangement is satisfactory although slightly nonlinear.

2.3 FORCE PLATE

The force plate is a large diaphragm-type pressure gage (Carlson-Wiancko, Reference 9) with a 7-3/8-inch-diameter sensitive area mounted in a 12-inch-diameter baffle. It was placed on the front of a tower head-on to the blast to measure total (or stagnation) pressure in a shock wave. More specifically, it was used to obtain the time variation of the head-on pressure of a mixture of dust and air on a sizeable object.

The finite size of the baffle causes edge effects which make the average pressure over the sensitive area slightly less than true stagnation pressure. For the plate dimensions, the correction is 5 percent of the air dynamic pressure when the flow is normal to the area (zero pitch and yaw angles); the correction is very nearly constant for flow having Mach

---

[1] We are indebted to E. H. Engquist of Chemical and Radiological Laboratories for providing us with particle-size data on a sample from Frenchman Flat.

Figure 2.1 Calibration of wind-direction gage used in the pitch sense (Shot 12).

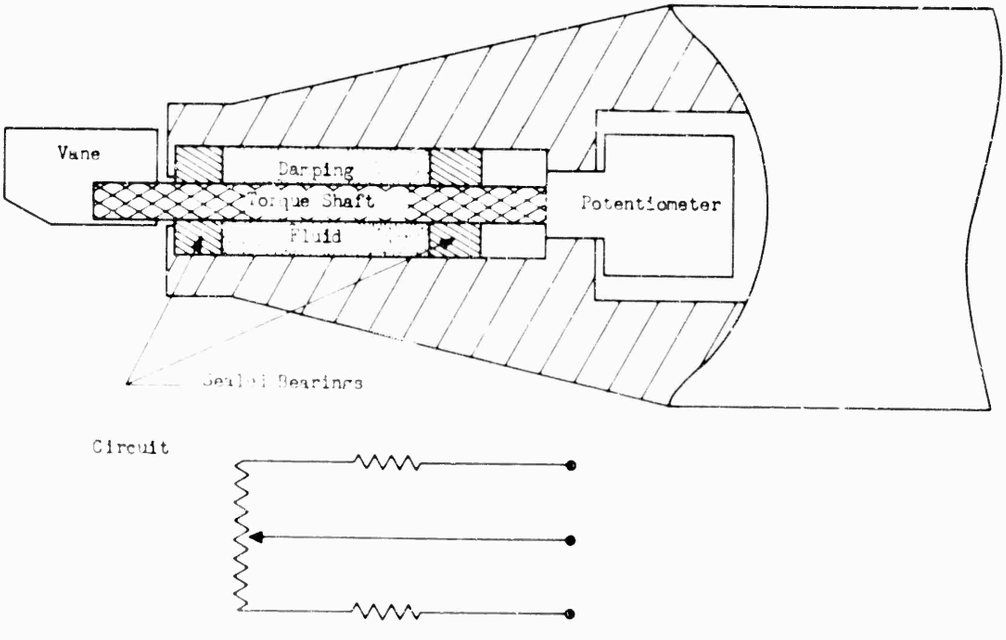

Figure 2.2 Schematic diagram of wind-direction gage.

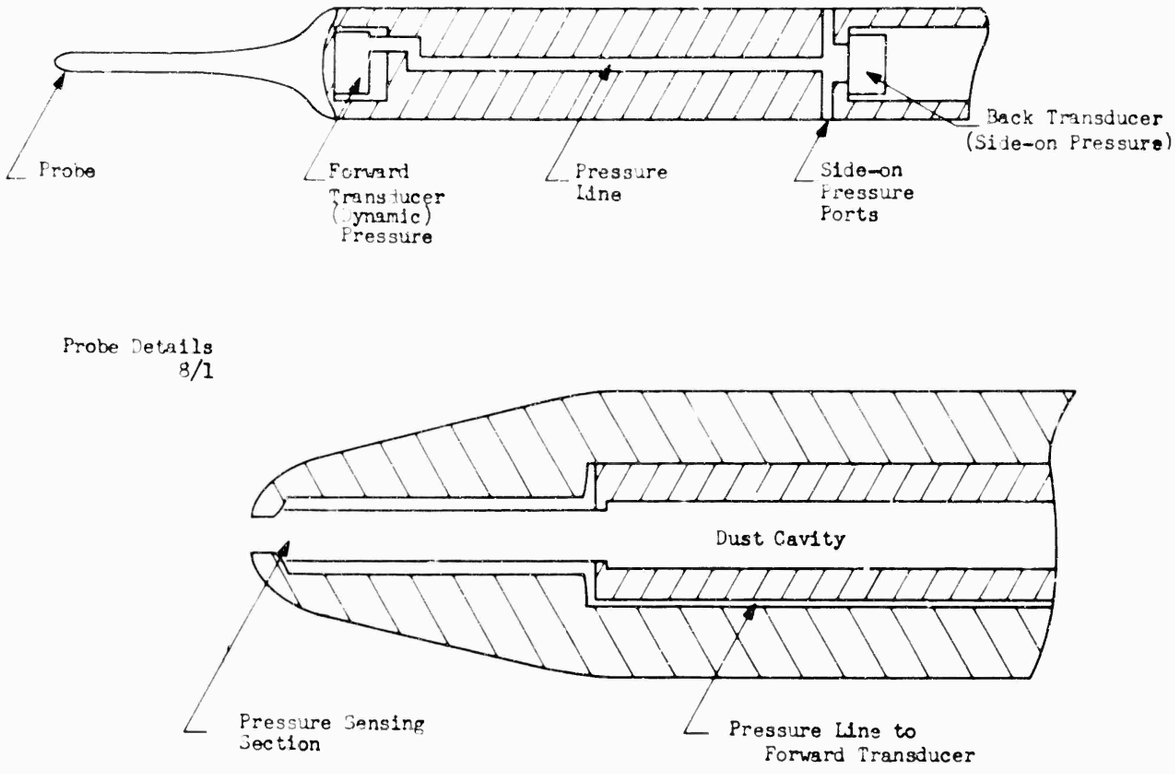

Figure 2.3 Schematic diagram of snob gage.

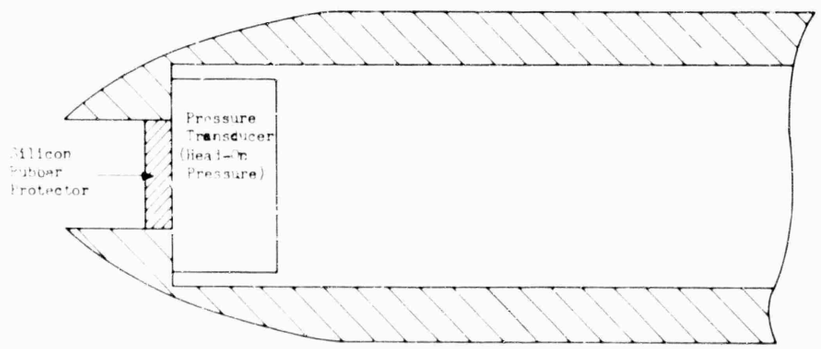

Figure 2.4 Schematic diagram of greg gage probe.

numbers between 0.25 and 0.8. For pitch (or yaw) angles other than zero, corrections are available from wind-tunnel data and are Mach-number sensitive.

Total pressure (P_t) is also recorded at the front end of an ideal pitot gage. Observed dynamic pressure of a compressible fluid (q_{ac}) is the difference between total pressure (P_t) and static (side-on) overpressure (ΔP). The usual pitot-static tube has a small sensing forward area, but size should make little difference for clean air. For dusty air, on the other hand, size of the obstacle affects the registering coefficient of dust. Use of the force plate allows one to examine the effect of obstacle size and provides a better index of the force that might be expected on the forward face of a large obstacle.

2.4 CENTRIPETAL-DENSITY GAGE (REFERENCE 10)

Developed to make a continuous measurement of air density from zero time throughout the passage of the shock wave, this gage was mounted at the center of a side-on 24-inch-diameter baffle. It is similar to the usual centripetal air pump and produces a high-velocity stream of air by a set of vanes rotating at about 24,000 rpm. Two stationary pressure probes are located at the periphery of the rotating column of air, one facing upstream and the other downstream. The difference in pressure between the two probes is directly proportional to the dynamic pressure imparted to the air column by the rotating vanes. The velocity of the air is constant, since it is imposed upon the air by constant speed vanes. This means differential pressure is proportional to the density of air in the gage. A continuous sample of free-stream shock-wave air is drawn in at side-on pressure; thus, differential pressure recorded by the gage is directly proportional to free-stream density of air in the shock wave. Before shock arrival, the gage should record changes in ambient density caused by development of the thermal layer.

The centripetal-density gage utilizes a diaphragm-type differential pressure transducer (Ultradyne) as the pressure detector for the two probes. A static pressure gage, using the same type of transducer, is mounted on the side-on baffle, giving static (side-on) overpressure at the same point and time that density measurements are made. Air temperature may be obtained by using overpressure and density data in the perfect gas equation.

Static tests in a variable-density and variable-temperature chamber show that the gage does read density, but wind-tunnel tests show some sensitivity to Mach number, probably caused by heating of the whole gage by air friction in the long steady-state runs of the wind tunnel; this sensitivity has never been manifest during full-scale shock waves.

Developed at Sandia Corporation prior to Operation Upshot-Knothole to measure the air density in a shock wave, exclusive of dust, the gage performed satisfactorily on Shots 1, 9, and 10 of Upshot-Knothole (Reference 5). Between Operations Upshot-Knothole and Castle the gage was modified by doubling the rotor speed and mounting in a smaller baffle; it operated

satisfactorily on each of two shots in Operation Castle (Reference 11). The model used in Operation Teapot was essentially the same as that used in Castle.

2.5 PARTICLE-VELOCITY GAGE (REFERENCE 12)

In the Frenchman Flat area, dust and air should have the same speed; for other areas, this gage, which was designed to measure particle velocity of air in a shock wave, should give the velocity of the faster of the two components. The significance of this measurement is apparent from Equation 1.1. Unfortunately no useful records were obtained as the gage was impaired by the zero transient.

Operationally, the gage determines the transit time of a small pulse of ions carried by the air stream over a known distance. This ion pulse is produced by applying a high-voltage pulse of 4-μsec duration to a sharp hardened steel emitter probe, thereby ionizing the air flowing past the point at that time. Transit time is determined by detector probes which are driven positive as the ion pulse passes them. The three detector probes are positioned over a 20-degree arc with the emitter probe at its center.

2.6 MEDIUM-DENSITY GAGE[1]

Unlike the centripetal-density gage, the medium-density gage was designed to register both air and dust; but primarily, it was used on Operation Teapot as a dust-density gage, since it would be possible to correct its response for the effect of air-density changes. No useful records were obtained, as the gage proved sensitive to thermal radiation. The principle of the gage is to use changes in the dielectric constant of the medium during passage of a blast wave to determine density. These dielectric-constant changes alter the capacitance of a sensing element consisting of two coaxial cylindrical plates. Variations of this capacitance change the resonant frequency of a tank circuit which includes the exposed capacitor. Output of the tank-circuit oscillator is beat against the signal from a fixed-frequency oscillator. Thus, variations in beat note are an index to the medium dielectric changes. This beat frequency was recorded directly on magnetic tape. The proposed analysis technique is discussed in Appendix B.

2.7 VALUE OF INSTRUMENTATION

Individually the instruments gave interesting records; however, the most useful and significant results were obtained by the use of a group of gages at each station, with all gages located at about the same height above the ground.

The ensemble-use of the instruments was to provide the following advantages: (1) Measurement of the individual factors which determine dynamic pressure should enable one to see which factors account for high dynamic pressures. (2) One could examine the flow direction history and effect of obstacle size on head-on dust loading. (3) Numerous cross-

[1] Developed by J. W. Valentine and T. G. Banks, Jr., of Sandia Corporation from a concept evolved by M. Cowan, Jr. and H. H. Sander of Sandia Corporation (Reference 13).

TABLE 2.1 BASIC EQUALITIES AND CROSS-CHECKS ON INSTRUMENTATION

For simplicity it is assumed that compressibility and individual instrument corrections have been applied.

Quantity	Symbol	Instruments
Overpressure	ΔP	Snob Back Transducer, Transducer in Centripetal Density Gage Baffle
Air Density	ρ_a	Centripetal Density Gage
Air Velocity	u_a	Particle Velocity Gage
Air Dynamic Pressure	q_a or $1/2\ \rho_a u_a^2$	Snob Forward Transducer
Dust Density	ρ_d	Medium-Density Gage
Dust Velocity	u_d	About the same as air velocity if particles small
Dust Dynamic Pressure	q_d or $\rho_d u_d^2$	Dynamic pressure of Greg minus Dynamic pressure of Snob
Head-On Pressure	$(P_t)_f$	Force Plate
Head-On Pressure	P_t or $P + q_a + q_d$	Greg Gage
Pitch	θ	Wind Direction Gage
Yaw	ϕ	Wind Direction Gage

Other Equalities

$$(P_t)_f = \Delta P + q_a + n\, q_d$$

Here n, which should be between one half and one, is a registering coefficient of dust on the Force Plate.

Quantity and Instruments		Quantity and Instruments
ΔP (Snob)		ΔP Pressure transducer located in density gage baffle
q_a (Snob)	Should Equal	$1/2\ \rho_a u_a^2$ (centripetal density gage and wind velocity gage)
q_d (Snob and Greg)		$\rho_d u_d^2$ (medium density gage and wind velocity gage)

The other possible cross-checks are obvious from these relations.

checks of instruments would be possible (Table 2.1). (4) It would be possible to infer quantities not measured because of instrument failure. (5) It would be possible to check the first three hypotheses about the cause of excessively high dynamic pressures.[1]

Finally, it can be said that the instrumentation of Project 1.11, except for flow-direction studies, did not give a complete coverage of the precursor phenomenon, since only two groups of gages were situated on each blast line. The experiment was basically an exploratory one, intended to check dust significance and to determine if a more complete examination was necessary and feasible.

[1] It must be admitted, however, that the check was considerably slanted to yield detailed information in the event that the dust-loading theory proved correct. The check between the first two hypotheses was actually better accomplished by the use of different surfaces employed on Shot 12.

Chapter 3

EXPERIMENTAL PROCEDURE

3.1 INSTRUMENTATION LAYOUT

Project 1.11 was primarily intended to instrument Shot 12. However, since most instruments were new, it was decided to give them a preliminary field test, which would have the further advantage (provided instruments operated satisfactorily) of giving dust load and precursor information from a different surface.

For this test (Shot 4), two 3-foot towers were situated side by side at a ground distance (2,150 feet) to approximately correspond (according to anticipated yields) to 2,000 feet on the desert line of Shot 12. One tower carried a particle-velocity gage, a centripetal-density gage, a force plate, and a wind-direction gage (mounted to measure yaw). The other carried a snob and a greg gage. At 1,350 feet from ground zero, a wind-direction gage was mounted in the pitch-sensitive position (Figure 3.1). Figure 3.2 shows the towers before and after Shot 4. The baffle of the centripetal-density gage was blown away; the structural weakness at fault was corrected in units used on Shot 12.

On each of the blast lines for Shot 12 (desert, asphalt, and water), twin 3-foot towers were located at ground distances of 2,000 and 2,500 feet. Mounted on each tower was the same array of gages used on Shot 4, except that the wind-direction gage was replaced with the medium-density gage on the desert line and neither gage was used on the other lines. Wind-direction gages were mounted to measure pitch. Only one particle-velocity gage (2,500 feet on the desert line) was used on Shot 12, since the check shot indicated that the gage was unreliable.

Most wind-direction-time measurements were for pitch (Table 4.1) at stations where Project 1.10 measured dynamic pressures.

Yaw-time measurements were made on the water line to check cross feed from the adjacent desert. Gages at 1,500 feet from ground zero were located 175 and 275 feet from the centerline, while those at 2,500 feet from ground zero were located 110 and 250 feet from the centerline. Yaw-time measurements were made on and beyond the water line at 2,650, 2,750, 3,000, 3,150, and 3,350 feet from ground zero for Project 5.5. These support measurements were supplemented by measurements of dynamic pressure at 2,650, 3,150, and 3,350 feet by use of pitot-static gages loaned by Stanford Research Institute.

Finally, on Shot 12, pressure- and dynamic-pressure-time records were obtained at 8,000 feet on the desert line to determine if the dynamic-pressure-time curve was different than would be expected over an ideal surface. Measurements were made with a pitot-static tube mounted at a height of 10 feet.

Figure 3.1a Wind-direction gage measuring pitch at 1350 ft on Shot 4 (preshot).

Figure 3.1b Wind-direction gage measuring Pitch at 1350 ft on Shot 4 (postshot).

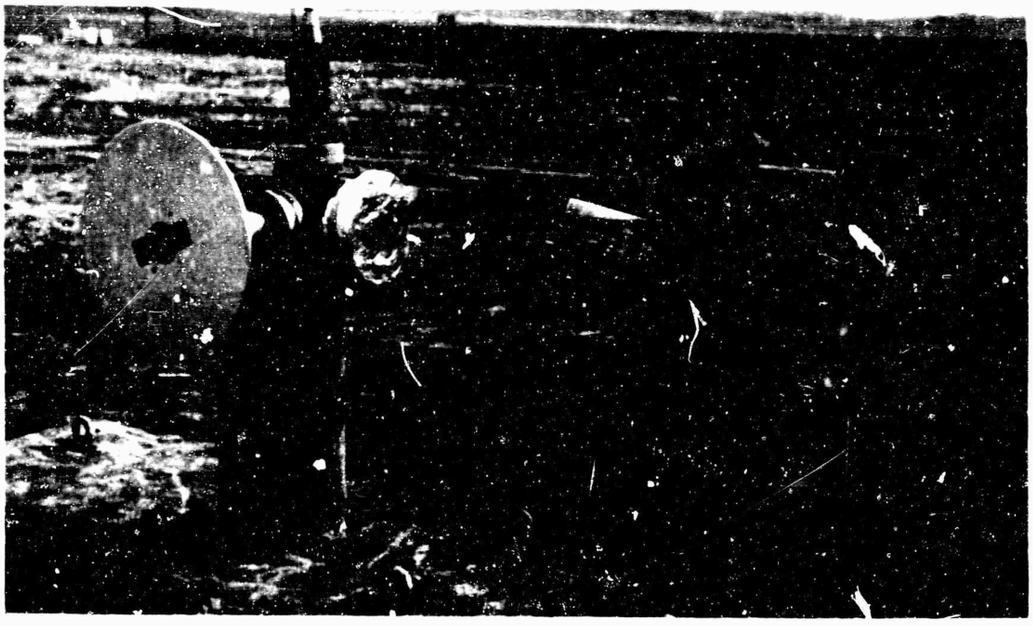

Figure 3.2a Towers with special dynamic pressure instruments (2150 ft from ground zero, pre-Shot 4).

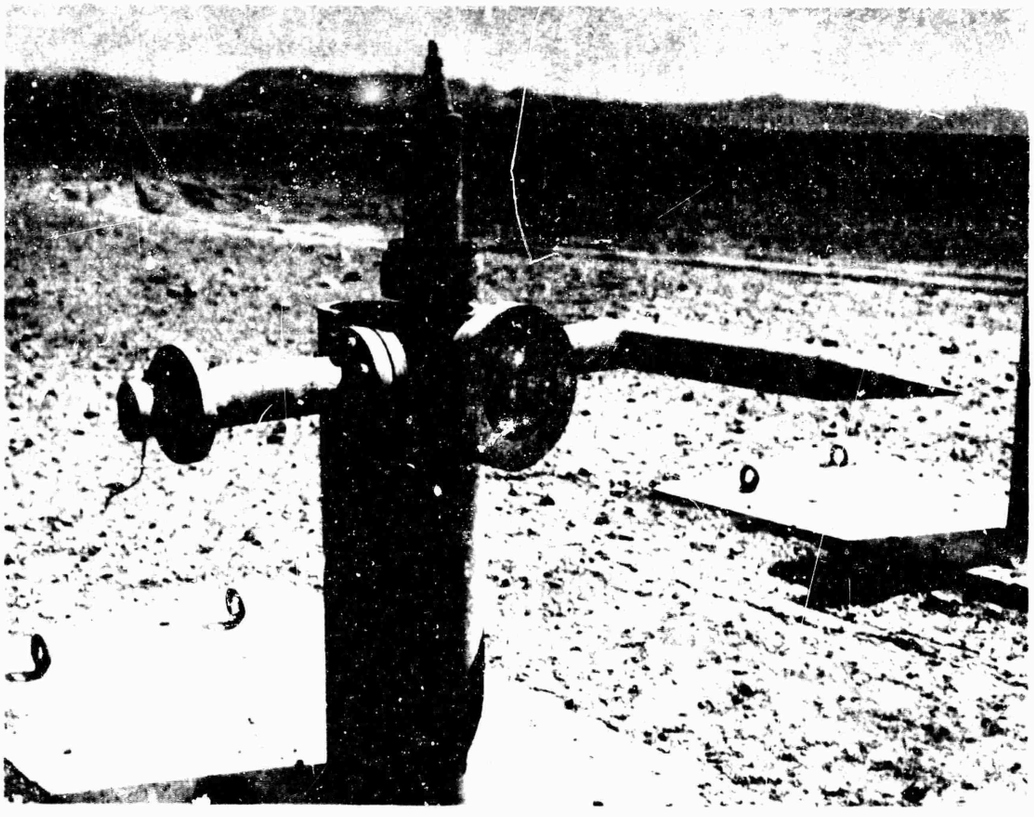

Figure 3.2b Foreground tower with "baffleless" centripetal-density gage, force plate, particle-velocity gage, and wind-direction gage (post-Shot 4).

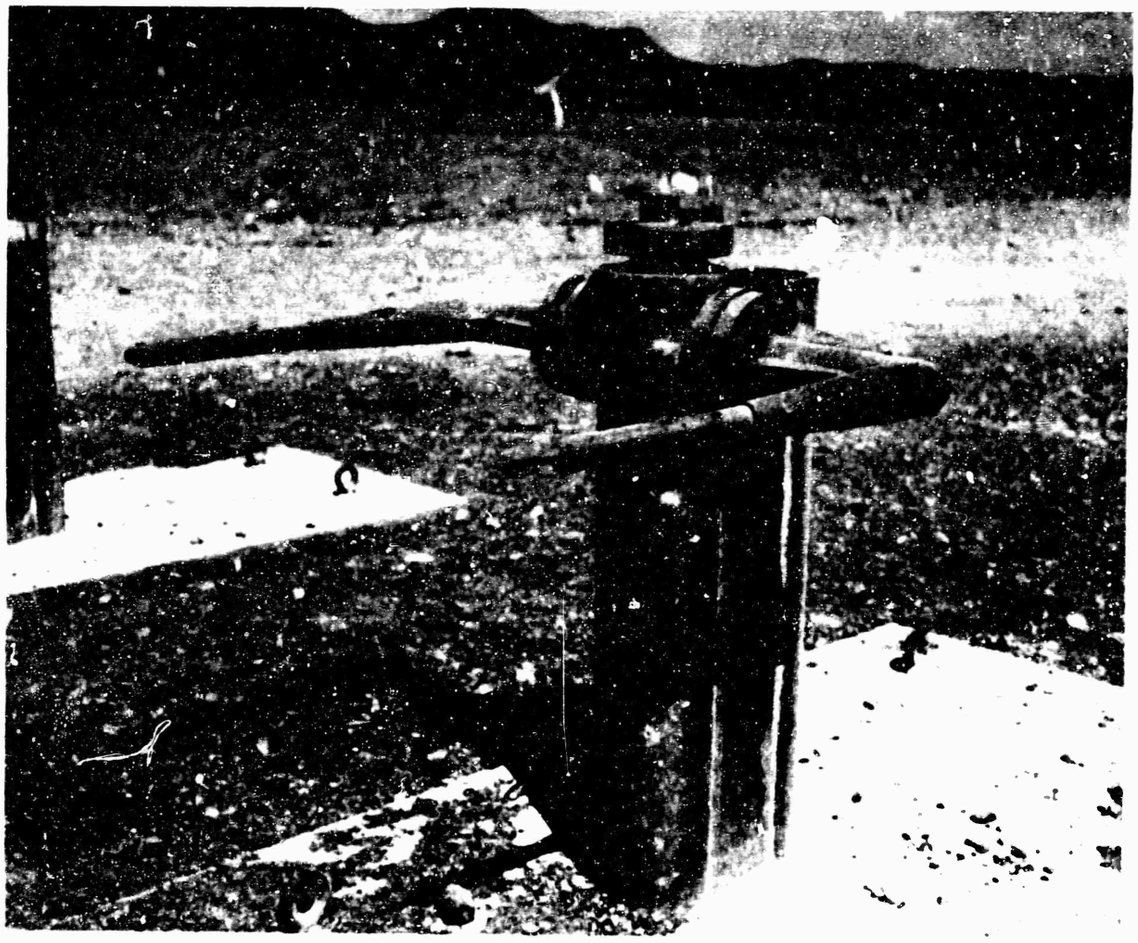

Figure 3.2c Background tower with snob and greg gages, and an unofficial dust sampler (post-Shot 4).

3.2 RECORDING SYSTEM

All instruments were used in combination with a new direct-current recording system developed by Sandia Corporation (Reference 14). To reduce loss of information, results were recorded in two ways: (1) by a direct-current signal recorded on photographic paper, and (2) by a frequency-modulated signal recorded on magnetic tape. Preshot checks determined that the methods agreed to within 1 or 2 percent; in data reduction, both types of records were used.

Chapter 4
RESULTS AND DISCUSSION

Operation Teapot Shot 12 was detonated April 15, 1955, at 1115 PST on a 400-foot tower in Frenchman Flat; the yield was estimated to be 24 kt. Geometry of the device was such that a symmetric explosion was expected.

During the shot all instruments remained in place; however, some sustained missile damage, particularly on the asphalt line. Records and postshot checks revealed that a number of gages had been burned out by the zero-time transient. This zero-time transient also reduced the value of information obtained from a few other gages by grossly changing their sensitivity. The particle-velocity and medium-density gages performed unsatisfactorily.

Despite these disappointments, a large amount of information was obtained, and the experiment is deemed successful.

4.1 DATA REDUCTION AND READING TECHNIQUES

For data evaluation, records were studied with a reading device which recorded time and deflection by punching a series of IBM cards. These times and deflections, with calibration data, formed the basis for an expanded plot from which parameters were read. A few records were so "hashy" that they were smoothed by averaging.

Since most records did not exhibit classical wave shapes, one had to be somewhat arbitrary in defining peak values. We chose to read only those values having durations of more than 5 msec, ignoring isolated spikes which exceed the defined maximums, since any signal of less than 5-msec duration has questionable damage and physical significance. Time of maximum is the time the deflection first achieves its maximum value.

For pitch measurements, however, the initial extreme value was read, whatever its duration, since we wish to study this type of maximum.

4.2 WIND-DIRECTION MEASUREMENTS

4.2.1 Pitch. Wind-direction gages performed satisfactorily except for those eliminated by the zero-time transient. Considerable pitch was observed on all lines, even over water where none was expected. Table 4.1 gives initial pitch information for the three lines. For desert and asphalt, Figures 4.4 and 4.5 give maximum initial pitch versus ground distance, and Figure 4.6 gives initial flow duration at various ground distances. Initial flow is considered finished either when the flow returns to horizontal or steadies to turbulent fluctuations about an average which is nearly horizontal.

From ground zero out to and including 2,250 feet on the desert and asphalt lines, pitch-time records show brief initial upward flow (positive

TABLE 4.1 INITIAL PITCH BEHAVIOR (θ), SHOT 12

Ground Distance	Surface	Gage Height	Time after Zero of First Vane Deflection	Max. Initial Pitch		End of Initial Period	Later Behavior and Remarks
				Value	Time after Zero		
ft		ft	sec	°	sec	sec	
1250	Desert	3					Gage out at zero
	Asphalt	3	0.184	+8.0	0.189	0.230	Settles on an average of +0.5°, shows a later maximum of +12° at 0.320 sec
	Water	3	0.245	+27	0.267	0.273	Goes to an average of -10°
1500	Desert	3					Gage out at zero
		10	0.271	+26	0.276	0.290	Settles to turbulent flow about +6°
	Asphalt	3					Gage out at zero
		10	0.249	+65	0.254	0.264	Settles to average about +9°
	Water	3	0.377	-20	0.437	0.498	Goes to +9°, flow nearly horizontal to 0.413 sec
		10	0.376	+18	0.418	0.432	After erratic period goes to an average on -8.5°
1750	Desert	10	0.350	+2.8	0.352	0.370	Sensitivity probably low
	Asphalt	10	0.326	+58	0.330	0.353	Settles on an average of +3°
	Water	10	0.495	-3.5	0.542	0.723	Goes to about +7°, extremely turbulent during negative pitch period
2000	Desert	3	0.457	+15	0.465	0.490	Goes to an average of -5°
		10	0.460	+36	0.467	0.510	Goes to an average of +6°
	Asphalt	3	0.422	+10	0.431	0.468	Goes to an average of -2.5°
		10	0.427	+44	0.437	0.480	Settles on an average of +1°
	Water	3	0.595	+14	0.618	0.626	Goes to an average of -2°
		10	0.607	-11	0.628	0.640	Goes to an average of +16°
2250	Desert	10	0.616	+51	0.635	0.712	Goes slightly negative, then back to +10°
	Asphalt	10					Gage out at zero
	Water	10					Gage out at zero
2500	Desert	3	0.815	+4.7	0.845	0.913	Goes to zero, then shows spike (+7°) finally goes negative
		10	0.837	+13	0.875	0.890	Goes to -7.5°, then steadies to -3.5°
		25	0.830	+13	0.933	0.965	Goes to -12°, then back to +6°
		40	0.835	+28	0.947	0.986	Goes to -10°, then back to +10°
	Asphalt	3	0.681	+6.5	0.691	0.799	Goes to an average of about -6°
		10	0.686	+18	0.708	0.924	Goes to an average of about -5°
		25	0.691	+22	0.720	0.821	Settles at +2° then goes to -10° at 0.950 sec
		40	0.700	+17	0.790	0.980	Goes to -10.5° after initial phase
	Water	10	0.895	+7.5	1.161		Flow nearly horizontal until 1.050 sec
2750	Desert	3	1.085	+5.9	1.343	1.390	Shows negative dip to -3° then goes back to +2°, shows plateau before initial peak
	Asphalt	3	0.835	+4.4	1.015	1.070	Settles to average about -1°, shows plateau before peak
	Water	3					Gage out at zero
3000	Desert	3					No detectable deflection
	Asphalt	3	1.041	+8.0	1.103	1.40	Settles at about +1°
	Water	3					Gage out at zero
3500	Desert	10					No detectable deflection
4500	Desert	3					No detectable deflection

pitch) after which flow is nearly horizontal (Figures 4.1 and 4.2). At the 3-foot level this steady, nearly horizontal flow is slightly downward (-) while at the 10-foot level it is usually slightly upward (+).

At 2,500 feet on these two lines, pitch begins with upward flow, which lasts considerably longer than at closer stations (Figures 4.1 and 4.2). This is followed by a period of downward flow in which the magnitude of negative pitch is comparable to that of the positive pitch before it. Downward flow lasts considerably longer on the asphalt than it does on the desert line.

Beyond 2,500 feet on these two surfaces, duration of initial upward flow increases while the tendency to downward flow after the initial phase is less pronounced or even lacking (Figures 4.1 and 4.2). At and beyond 3,000 feet on the desert line no pitch was observed. On the asphalt line, pitch was appreciable out to the last station at 3,000 feet.

Pitch-time records for the water line are given in Figure 4.3.

In Figures 4.4 and 4.5 maximum initial pitch obtained on the desert and asphalt lines are compared with maximum pitch of flow inferred from photographic and time-of-arrival data.[1] On the asphalt line at the closer stations, agreement between measured and estimated pitch at the 10-foot level is remarkably good. This means that these higher gages upon being enveloped by the shock were effectively above the thermal layer, for in this layer one would expect to observe a pitch less than that estimated. Apparently the thermal layer was thicker on the desert line since no such agreement was obtained between measured and estimated pitch. All measured pitches at the 10-foot level were less than estimated, except at 2,250 feet from ground zero.

Maximum initial pitch on the desert and asphalt lines was invariably less at the 3-foot than at the 10-foot level. This seems to confirm that flow must become horizontal as one approaches the surface (see Section 1.2).

In Figure 4.6, initial upward flow durations on desert and asphalt appear to increase with ground distance. There is also a marked tendency for the initial flow to persist longer at 10-foot than at 3-foot elevations. Finally, there is a slight tendency for the initial flow to last longer over asphalt than at corresponding stations over desert.

If correlation is attempted between initial upward flow durations and the delay between precursor and "main shock" arrival (here chosen as arrival times over the water) for the two lines, results are disappointing. The delay between shocks is much longer than the initial flow duration at closer stations, about the same at 2,500-foot stations, and less than initial flow durations beyond 2,500 feet.

Pitch-time behavior over desert and asphalt lines at 2,500 feet is given in Figures 4.7 and 4.8, where vectors representing the direction and magnitude of flow at various elevations are sketched at 50-msec intervals. It is tempting to consider the flow configuration a steady one passing the station and so specify a separation in distance as well as time between the various stages. Such a concept is misleading, since this flow configuration is a rapidly changing one induced by a pressure wave interacting with a thermal layer. Figures 4.7 and 4.8 show graphically that

---

[1] Flow angles were computed from the preshock speed of sound estimates listed in ITR-1153 (Reference 2). These angles apply above the thermal layer.

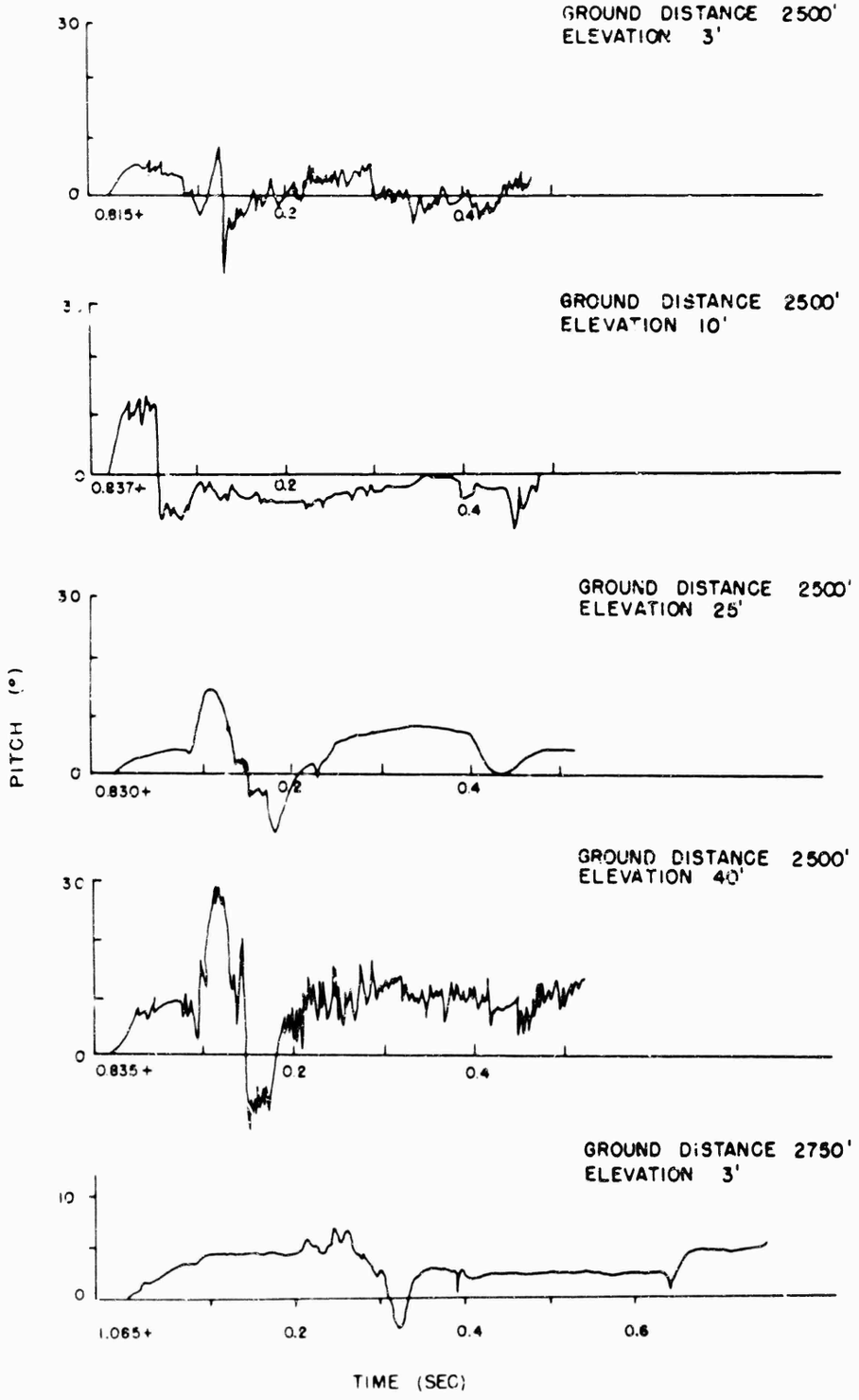

Figure 4.1 Pitch time records on desert line (time scale starts on signal arrival).

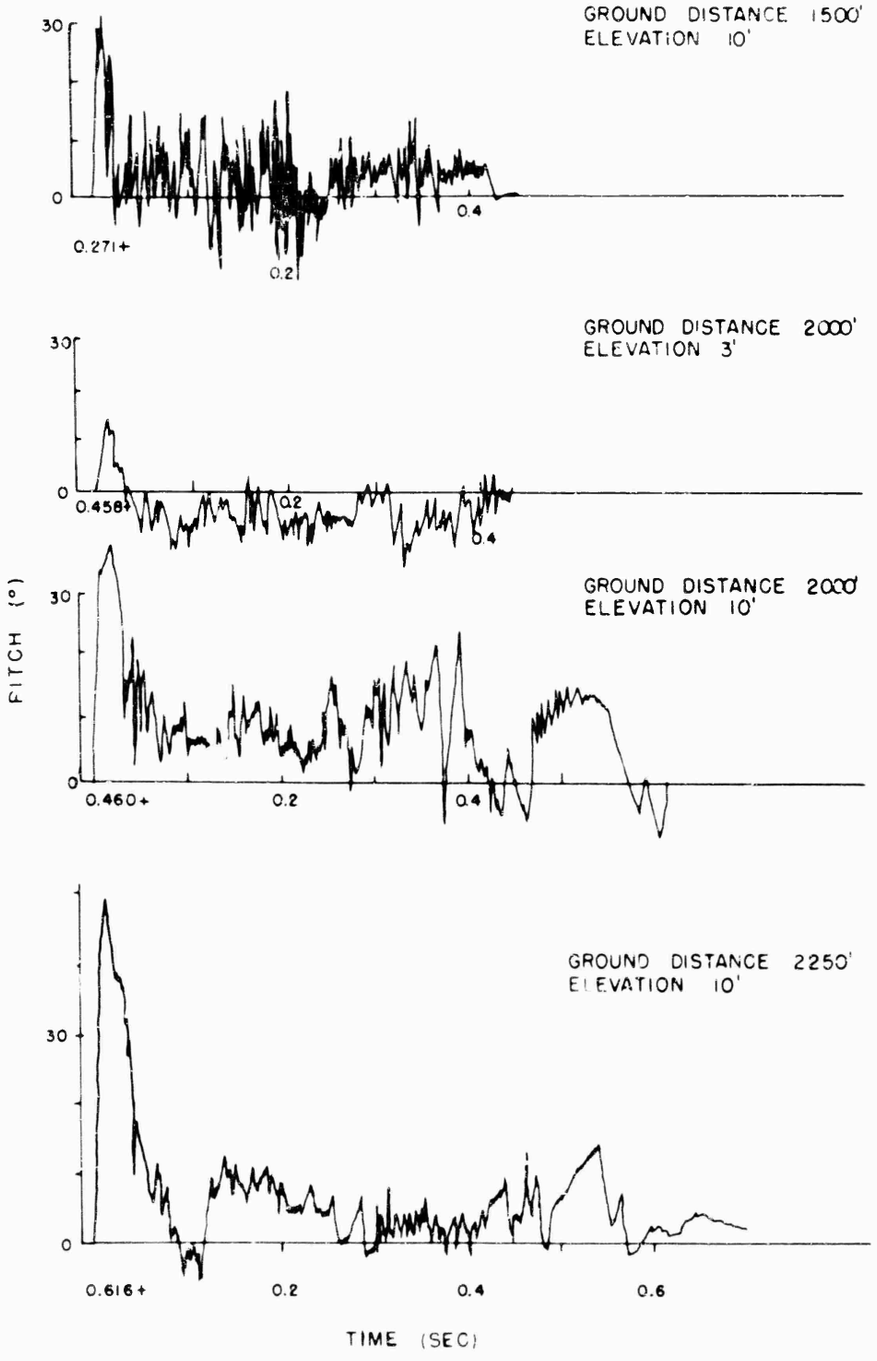

Figure 4.1 (Cont'd) Pitch time records on desert line (time scale starts on signal arrival).

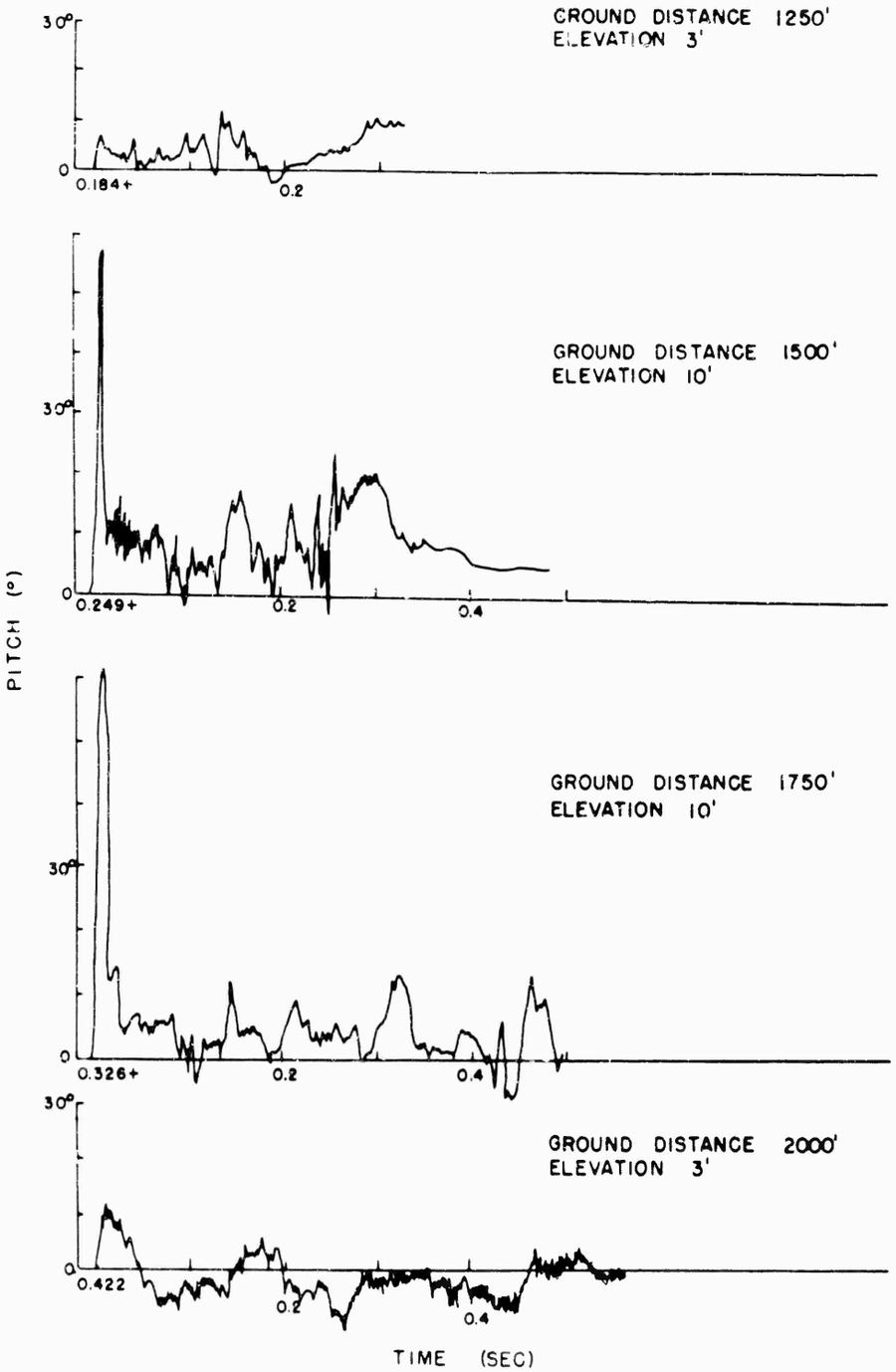

Figure 4.2 Pitch time records on asphalt line (time scale starts on signal arrival).

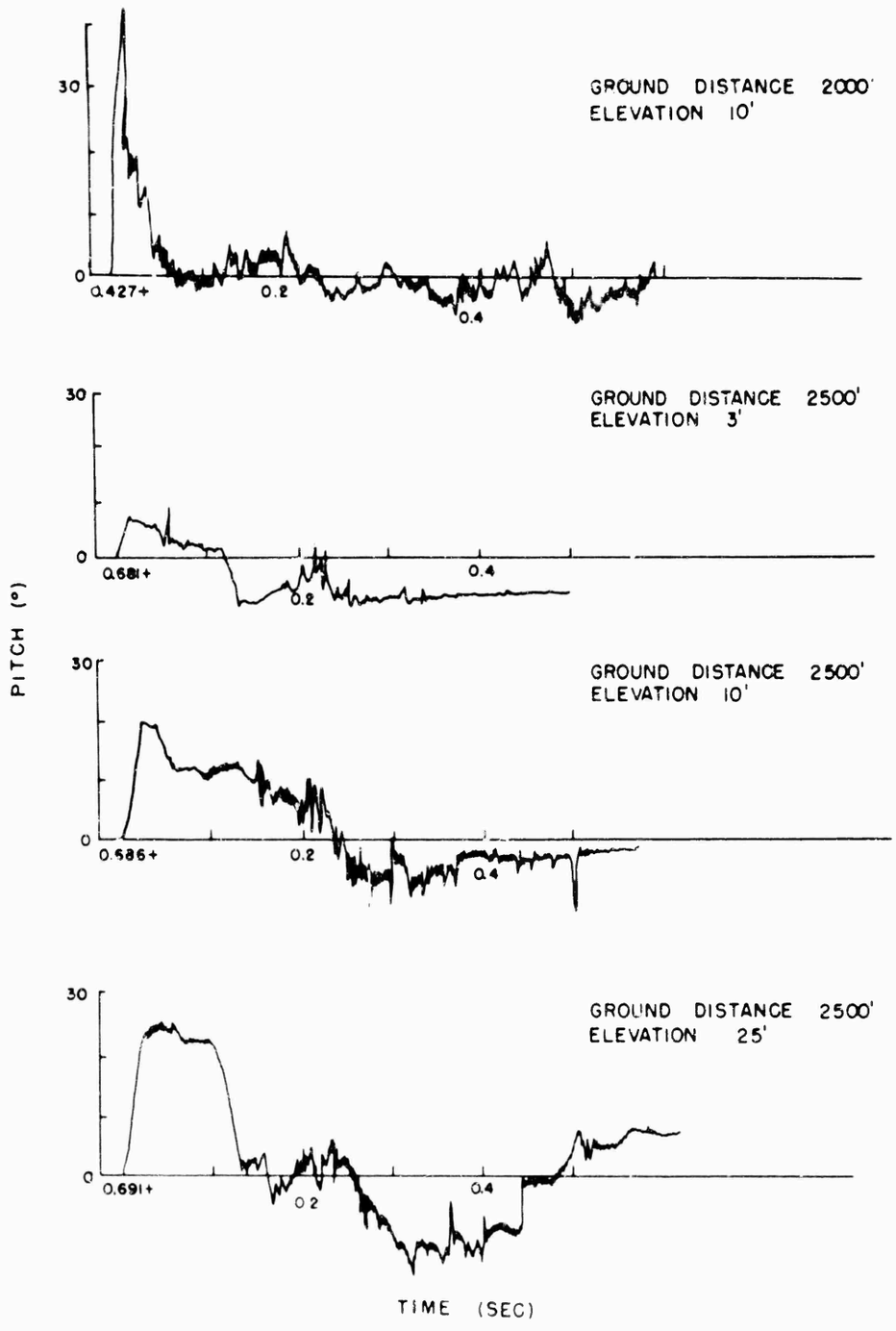

Figure 4.2 (Cont'd) Pitch time records on asphalt line (time scale starts on signal arrival).

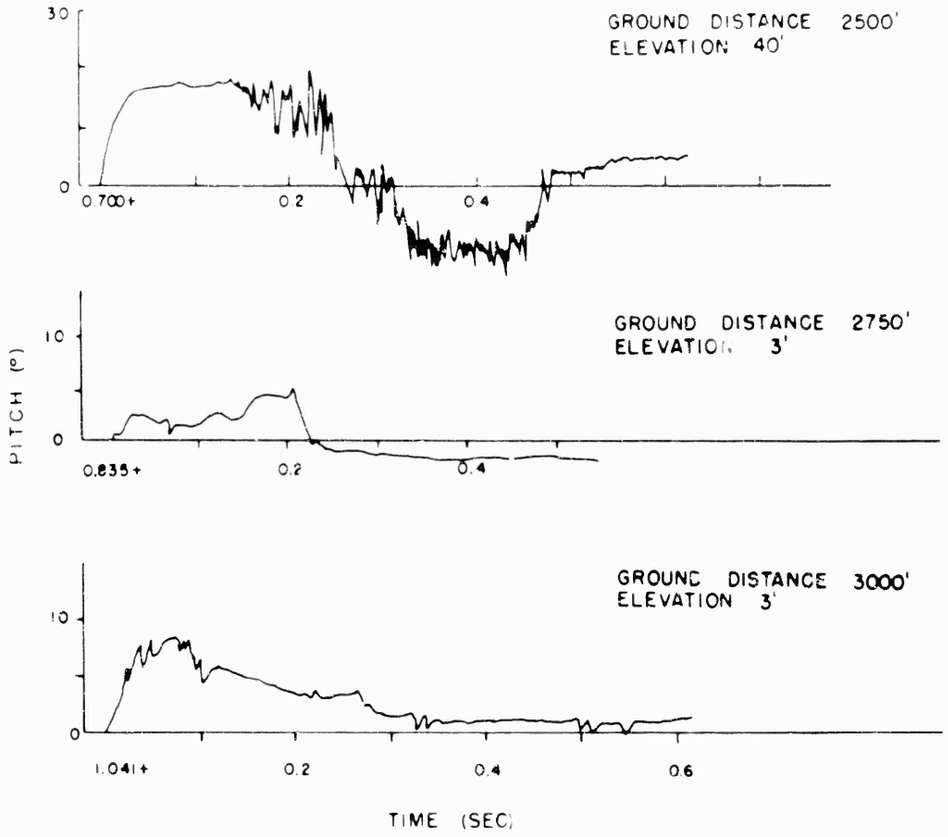

Figure 4.2 (Cont'd) Pitch time records on asphalt line (time scale starts on signal arrival).

downward flow at the 2,500-foot stations on the two lines begins at about the same time, namely 1 second. This is about 100 msec after shock arrival on the water line and suggests that the downflow represents "feed-through" from the shocked sphere of air above the precursor. Substantiating this, the desert line at the 2,500-foot station experiences its highest overpressure at this time and overpressure-time records on the asphalt show a plateau prior to the downward flow period. Perhaps even more significant, maximum air dynamic pressure occurs just prior to downward flow on the desert, while on the asphalt line air dynamic pressure is sustained at nearly a constant value until the downward flow period.

While pitch-time behavior was systematic over the desert and asphalt, it was not over water. Often the two elevations at a single ground distance have maximum initial pitches of opposite sign, although not at the same time. While the pitch behavior is erratic, compensating flows are usually present; that is, a period of one of pitch is followed by a period in which pitch has the opposite sign. The only apparent explanation of these records is that they represent a large-scale turbulence in the shock afterflow.

Little pitch was observed at the 1,750-foot station; there also the overpressure-time curve was nearly ideal. Likewise at 2,500 feet, where the overpressure wave again was nearly ideal, little pitch was observed

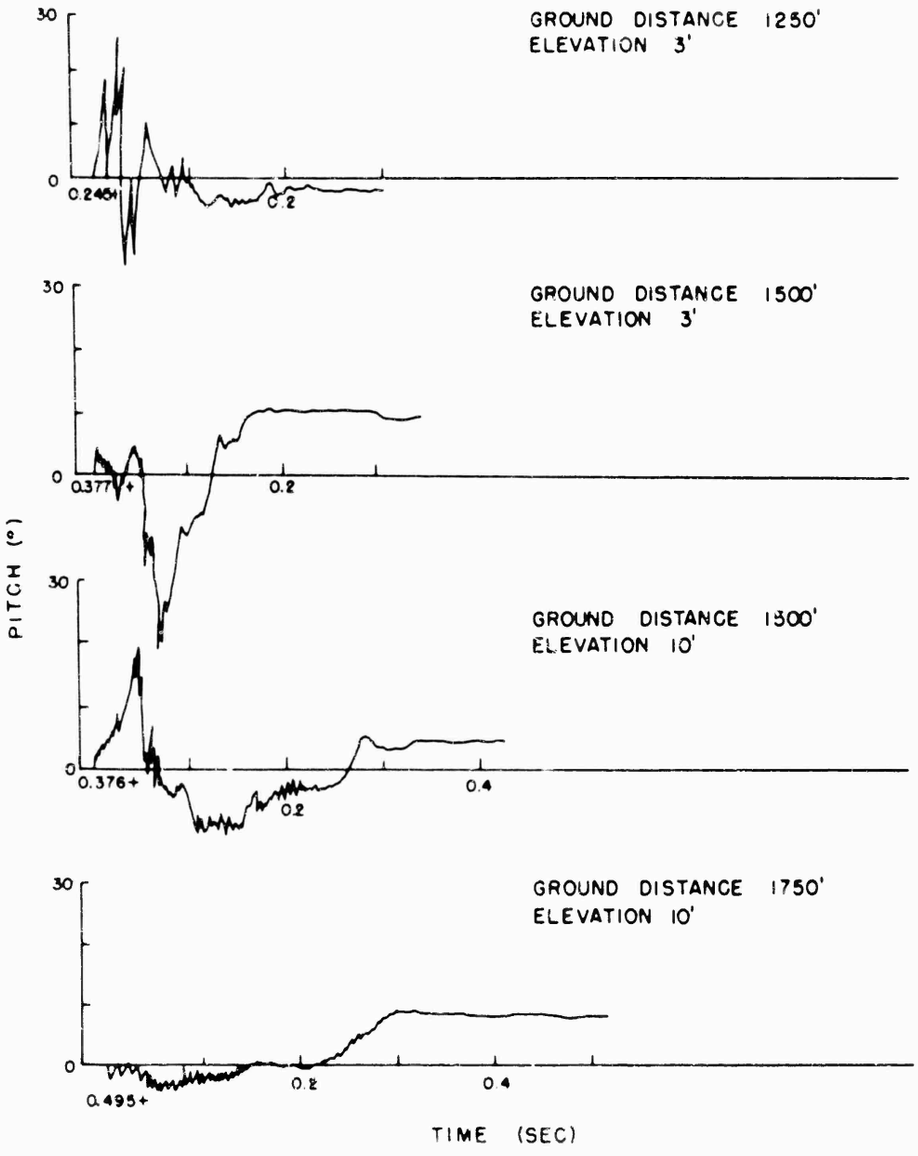

Figure 4.3 Pitch time records on water line (time scale starts on signal arrival).

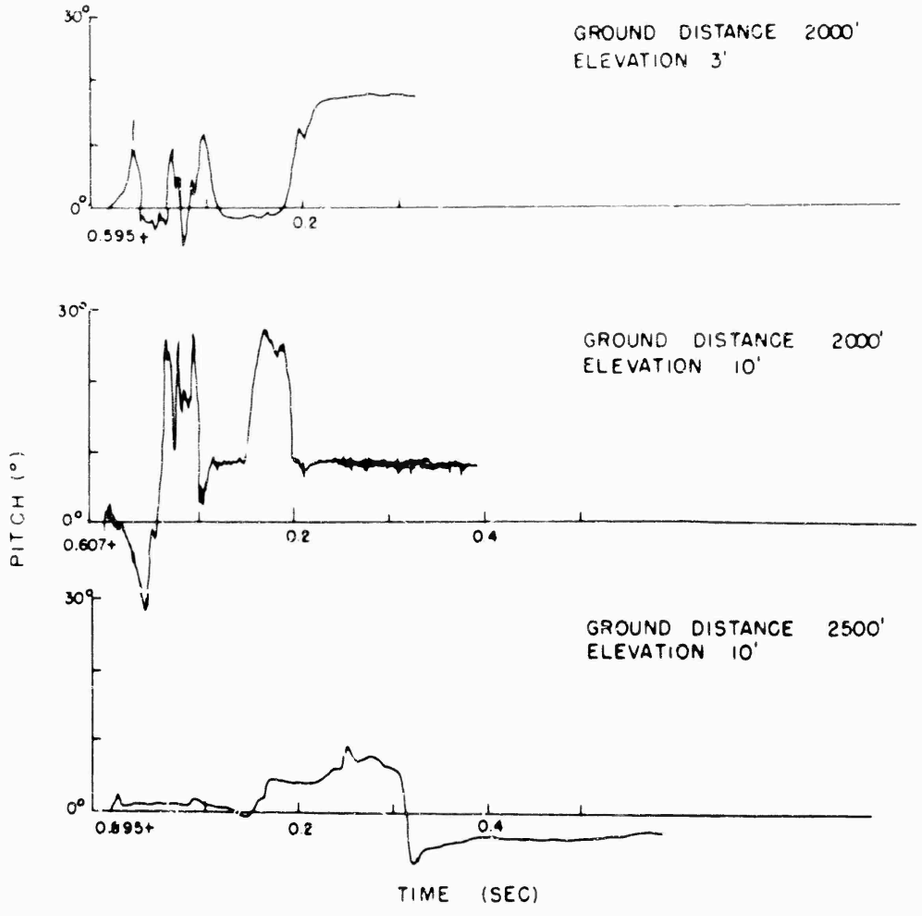

Figure 4.3 (Cont'd) Pitch time records on water line (time scale starts on signal arrival).

until about 100 msec after shock arrival after which a pitch-time pattern similar to those observed on the other lines at this distance was observed.

It was hoped that photography of the shock over the water line might clarify pitch behavior, but no satisfactory motion pictures were obtained because the shock wave over this line was screened by dust raised over the adjacent desert.

4.2.2 Yaw. Both instruments at the 1,500-foot station on the water line were burned out by the zero transient. Instruments at 2,500 feet, which were at 110 and 250 feet from the center of the 800-foot-wide blast line, showed no significant systematic yaw. The gage at 110 feet from the center displayed considerable erratic fluctuation (up to 67 degrees) well after shock arrival. This may have been caused by the passage of a cell of turbulence, or more likely, by mud striking the vane.

Yaw measured on the water line and beyond it for Project 5.5 was small, amounting to a degree or less. Maximum dynamic pressures measured at three of these stations are listed in Table 4.2.

Although no systematic yaws were measured over the water line, times of arrival at instruments stationed at 2,000 feet indicate that the first pressure signal came from the side with a considerable angle to the radius

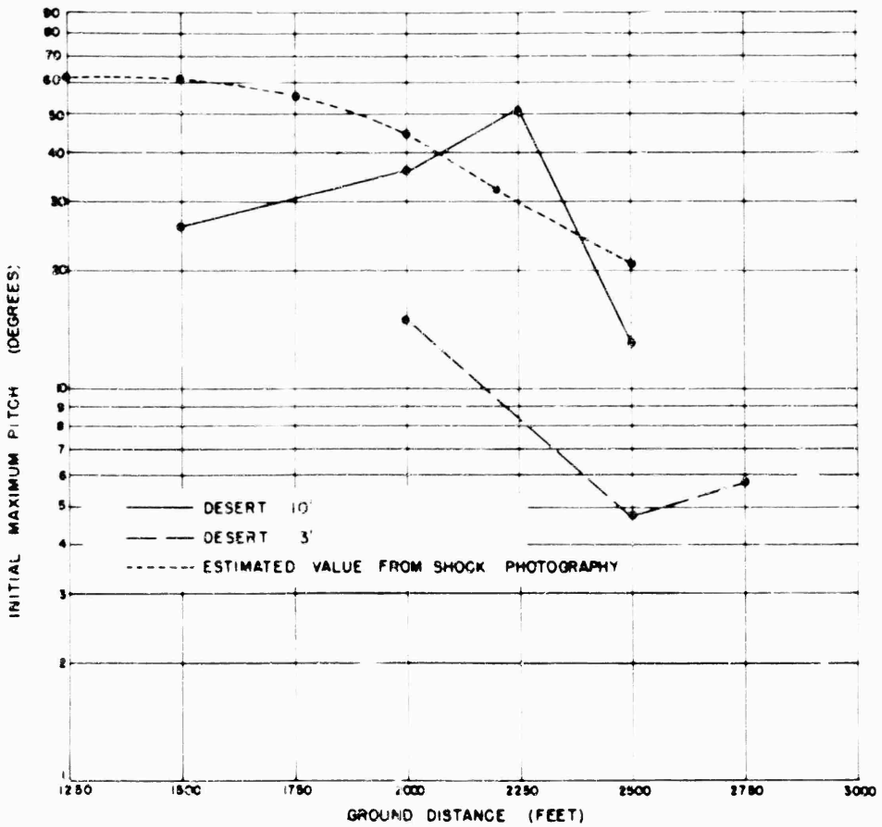

Figure 4.4 Maximum initial pitch versus ground distance (desert).

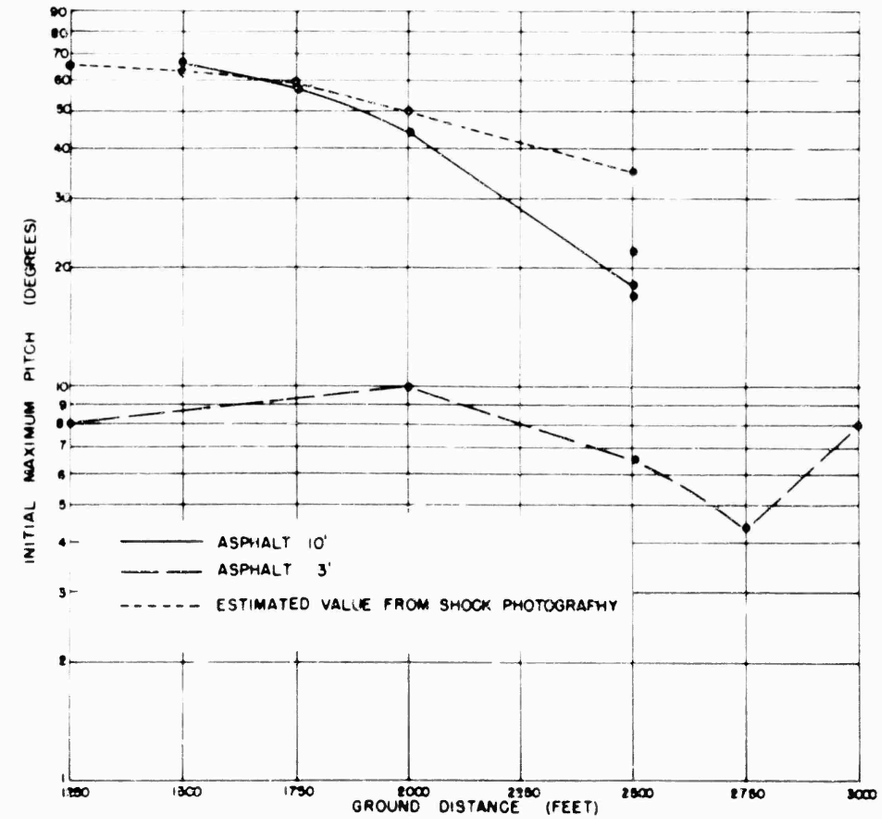

Figure 4.5 Maximum initial pitch versus ground distance (asphalt).

vector, perhaps as much as 40 degrees. The initial behavior of the instruments suggests the same result.

4.3 OTHER MEASUREMENTS

4.3.1 Snob and Greg (Air and Dust Dynamic Pressures). For this report it will be assumed that the snob gage registered no dust dynamic

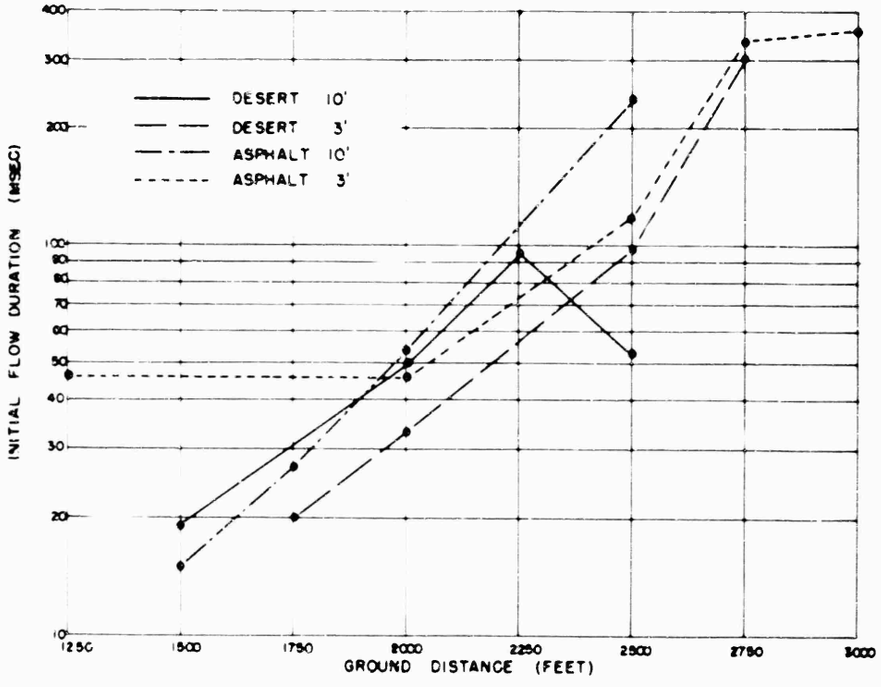

Figure 4.6 Duration of initial upward flow period as a function of ground distance (desert and asphalt).

pressure while the greg gage registered dust dynamic pressure ($\rho_d u_d^2$) fully. If substantial corrections are necessary because of the small size of the Frenchman Flat particles, an addendum giving these corrections will be published. However, the mean-mass particle diameter ran larger than expected so the correction will probably be small. In brief, the correction will be that air dynamic pressures given in this report will be somewhat high and dust dynamic pressures will be somewhat low.

Except for their vulnerability to missiles, these gages were satisfactory. Greg gage suffered considerably from missiles; one at 2,000 feet on the desert line and both gages on the asphalt line were impaired. Snob gages fared better, although the probes were partially sealed by late mis-

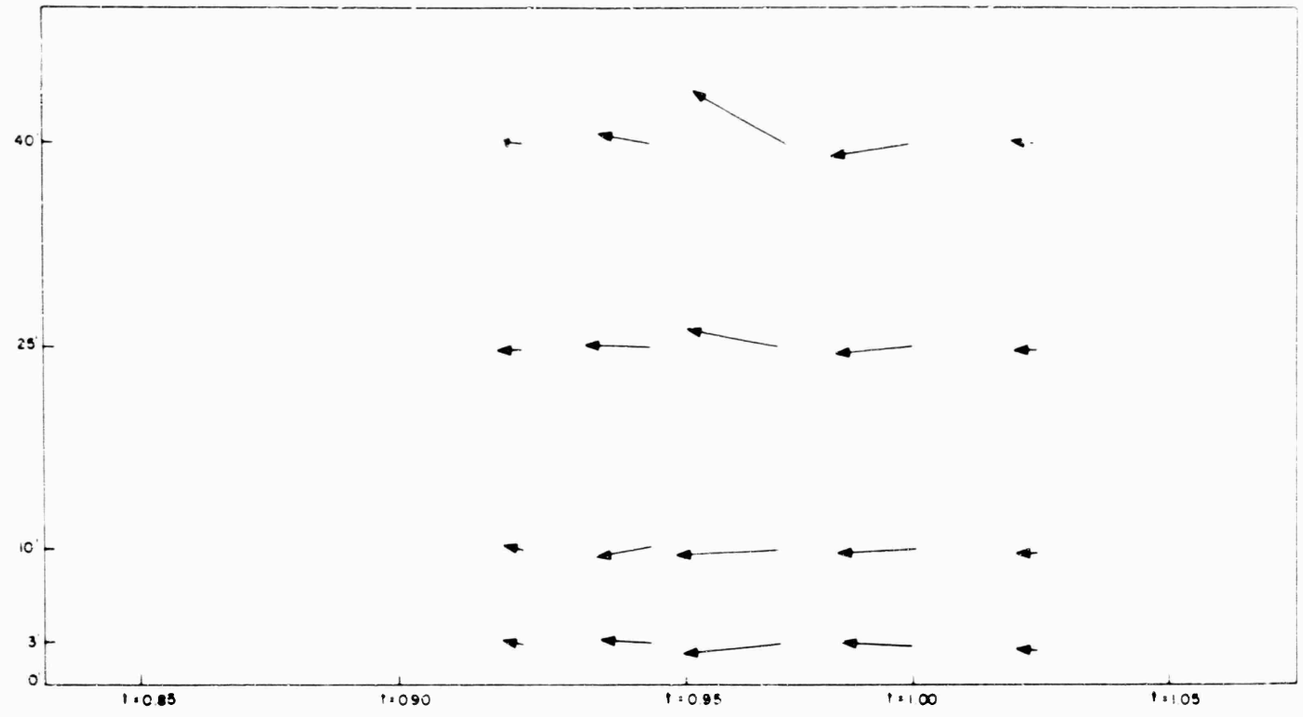

Figure 4.7 Pitch time history for various levels at 2,500 ft (desert), (length of arrows is proportional to estimated flow speed).

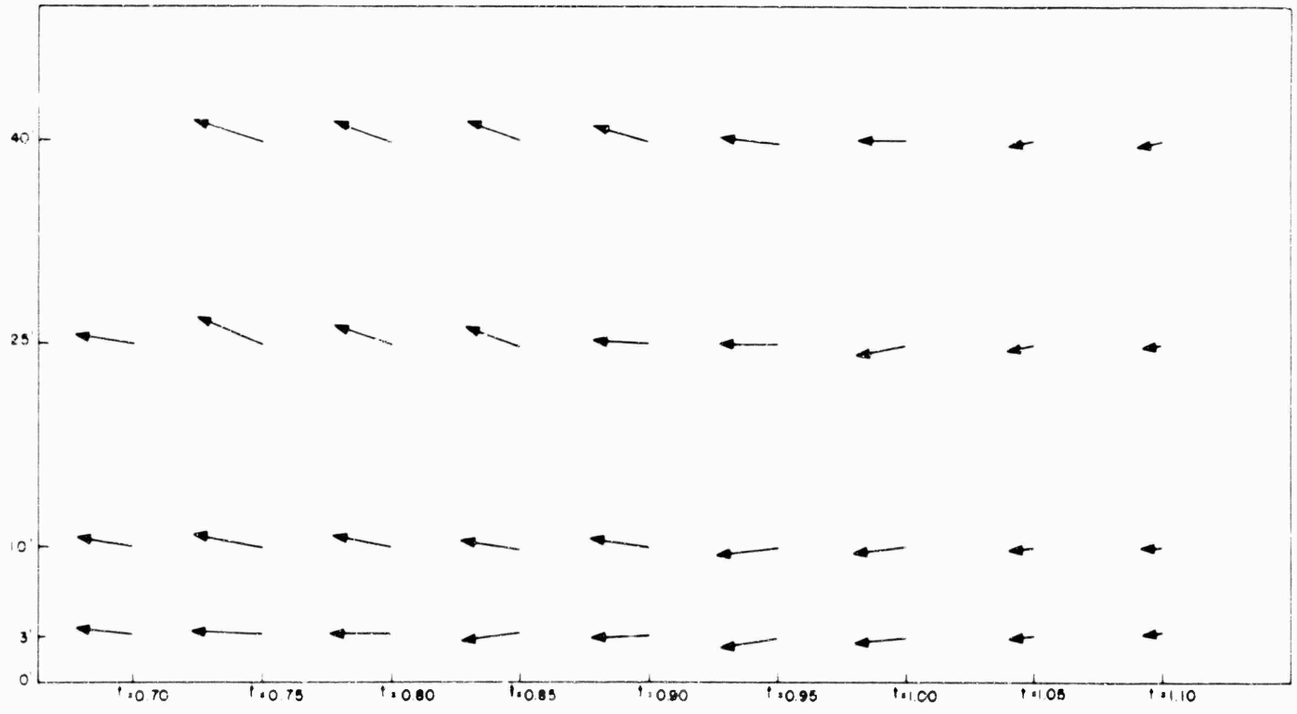

Figure 4.8 Pitch time history for various levels at 2,500 ft (asphalt), (length of arrows is proportional to estimated flow speed).

siles or mud; only the gage at 2,000 feet on the asphalt line lost information.

Peak values for the two instruments are listed in Tables 4.3 and 4.4, while records are displayed in Figures 4.9 through 4.14. Peak values of air dynamic pressure (snob differential) have not been corrected for Mach effects. The more academic corrected peak values of air dynamic pressure are given in Remarks of Table 4.3. Where Mach corrections were applied we have also corrected for the error in side-on pressure.

Air dynamic pressure-time records corrected for Mach effects are given in Figures 4.15 through 4.19. These corrections have been obtained by solving the equation

$$q_a = \frac{1}{2}\rho_a u_a^2 = \rho_a c^2 \left(\left(1 + \frac{2q_{ac}}{\rho_a c^2} \right)^{1/2} - 1 \right) \qquad (4.1)$$

where c is the local speed of sound. This expression is a rephrasing of Equation 1.3 retaining only the first two terms.

Equation 4.1 is somewhat misleading in that while ρ_a and c^2 may be individually obtained from air-density-time records their product is independent of air density. Instead $\rho_a c^2$ is proportional to absolute side-on pressure and Equation 4.1 may be written as

$$\frac{M^2}{2} = \left(\left(1 + \frac{2q_{ac}}{\gamma(P_o + \Delta P)} \right)^{1/2} - 1 \right) \qquad (4.2)$$

where M is Mach number and γ is the specific heat ratio. For the range of Mach numbers we are concerned with these expressions are effectively equivalent to the rigorous ones relating Mach number, observed dynamic pressure, and absolute side-on pressure. Computational errors incurred are less than those of measurement and less questionable than the uncertainties of applying analysis of a clean air case to the dusty afterflow of the desert line.

Dust dynamic pressure-time curves (q_d) are given in Figures 4.15 through 4.19. This quantity is derived by subtracting from the greg reading the uncorrected air dynamic pressure (snob) and the overpressure as registered by the snob side-on. For the water line at 2,000 feet from zero, the snob side-on pressure showed a short positive phase so the baffle side-on pressure was used after the maximum.

Peak air dynamic pressures at equal distances were highest over the desert, less high over asphalt, and lowest over water at both 2,000- and 2,500-foot stations. Only at 2,500 feet on the water line did the peak air dynamic pressure agree with the Rankine Hugoniot relations (Equation 1.2). This station experienced a nearly classical overpressure wave shape. At all other stations air dynamic pressure was higher than would be expected from measured overpressure and Equation 1.2, usually by a substantial factor.

Whitener has pointed out that Equation 1.2 is not truly applicable for computation of air dynamic pressure within an isentropic expansion

TABLE 4.2 PITOT STATIC TUBE DYNAMIC PRESSURE RESULTS (q'), SHOT 12

Ground Distance	Elevation	Surface	Time of Arrival	Maximum		Remarks
				Value	Time	
ft	ft		sec	psi	sec	
2625	6	Water	0.997	3.4	1.000	Some ringing
3150	6	Behind water line	1.346	2.0	1.346	Considerable ringing
3350	6	Behind water line	1.487	1.75	1.487	Considerable ringing
8000	10	Desert	5.304	0.056	5.304	

TABLE 4.3 SNOB RESULTS (q_{ac}), SHOT 12
(All Gage Elevations 3 ft)

Ground Distance	Surface	Time of Arrival	Max. Dynamic Pressure		Remarks
			Value	Time	
ft		sec	psi	sec	
	Desert	0.453	25 31	0.498 0.765	First maximum value corrected for Mach effect is 20 psi
2000	Asphalt	0.418	10.4	0.441	Gage was probably sealed by missile at maximum
	Water	0.596	6.1	0.695	Maximum value corrected for Mach effect is 5.8 psi
	Desert	0.786	8.4	0.945	Maximum value corrected for Mach effect is 7.5 psi
2500	Asphalt	0.676	6.2	0.740	Maximum value corrected for Mach effect is 5.8 psi
	Water	0.915	4.0	0.932	Maximum value corrected for Mach effect is 3.94 psi

TABLE 4.4 GREG RESULTS (P_t), SHOT 12
(All Gage Elevations 3 ft)

Ground Distance	Surface	Time of Arrival	Maximum		Remarks
			Value	Time	
ft		sec	psi	sec	
	Desert	0.452	68	0.503	Gage injured by missile at about 0.73 sec
2000	Asphalt	0.418	26.0	0.438	Maximum last valid value, gage was injured by missiles
	Water	0.596	7.9 18.7	0.598 0.692	Shows narrow spike to 24 psi at 0.640 sec
	Desert	0.786	26.7	0.936	
2500	Asphalt	0.675	13.5	0.699	Maximum last valid value, gage was injured by missiles
	Water	0.914	16.7	0.914	

having spherical symmetry (Reference 6). Possible corrections of Equation 1.2 for geometrical effects are discussed in Appendix C.

Dust dynamic pressures (Figures 4.13 through 4.19) were found to be substantial over the desert line, in fact the peak values of dust dynamic pressure exceed those of air at both the 2,000- and 2,500-foot stations.

Some dust[1] dynamic pressure was present over the asphalt surface but the amount was not determined, since gages at both stations were injured by missiles early in blast wave history. From combined snob and force-plate results one may infer the initial dust dynamic pressure was not very high, amounting at most to one psi at 2,500 feet on the asphalt line.

There was little or no such effect on the water line until late in the blast wave history. Finite dust[1] dynamic pressures are displayed late in the blast wave, but since these represent the differences of small quantities they are probably not significant. This does not mean that no water was present. Instead, the water, if present, was evaporated or broken into such small particles that it behaved essentially like air.

A dynamic pressure-time record was obtained at 8,000 feet on the

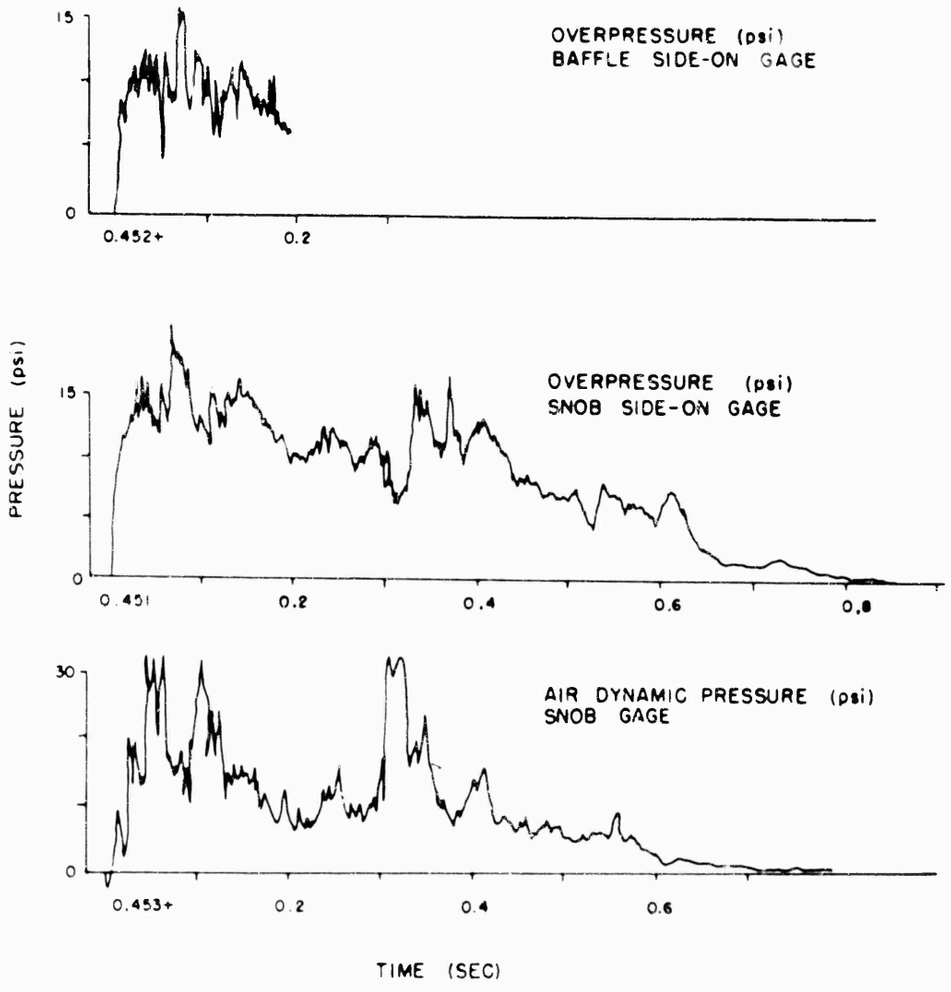

Figure 4.9 Time records of gages at 2,000 ft on the desert line (all gage elevations 3 ft, time scale starts on signal arrival).

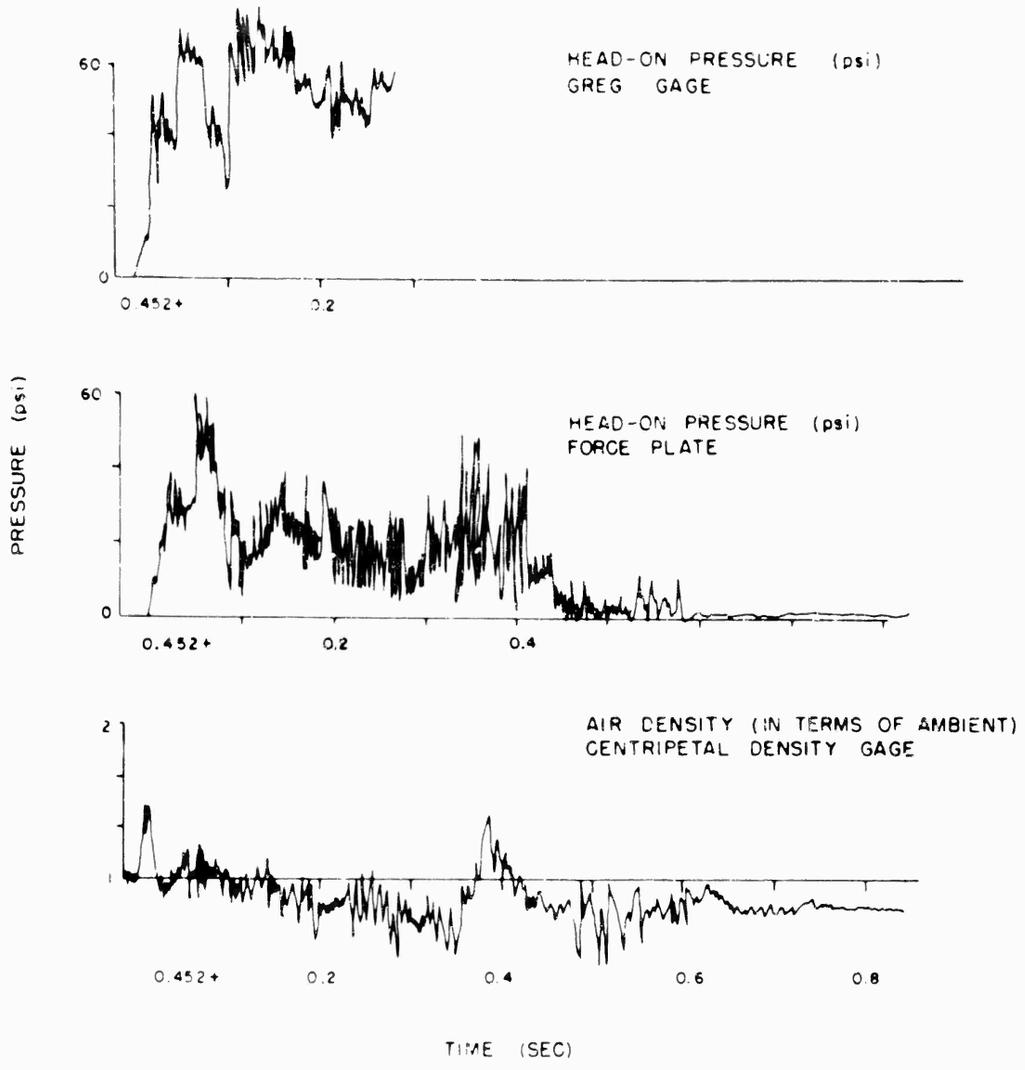

Figure 4.9 (Cont'd) Time records of gages at 2,000 ft on the desert line (all gage elevations 3 ft, time scale starts on signal arrival).

desert line; it showed no anomalous aspects and the peak value was in agreement with the Rankine Hugoniot relations.

4.3.2 Force Plate. Except for a marked tendency to show abnormally short positive phases, the force plate performed satisfactorily. The tendency may be a result of the effect of thermal (after shock arrival), missiles, or perhaps a leak at the back of the gage; whatever the cause, it means that late head-on pressures were often low. Results are listed in Table 4.5. Figures 4.9 through 4.14 show head-on pressure-time curves recorded at the various stations.

Since the force plate was a sizeable object, the flow of dust about it was expected to be more like air than it is around a small object, such as the greg gage. To check this hypothesis the sum of side-on pressure, air dynamic pressure, and half the dust dynamic pressure have been plotted

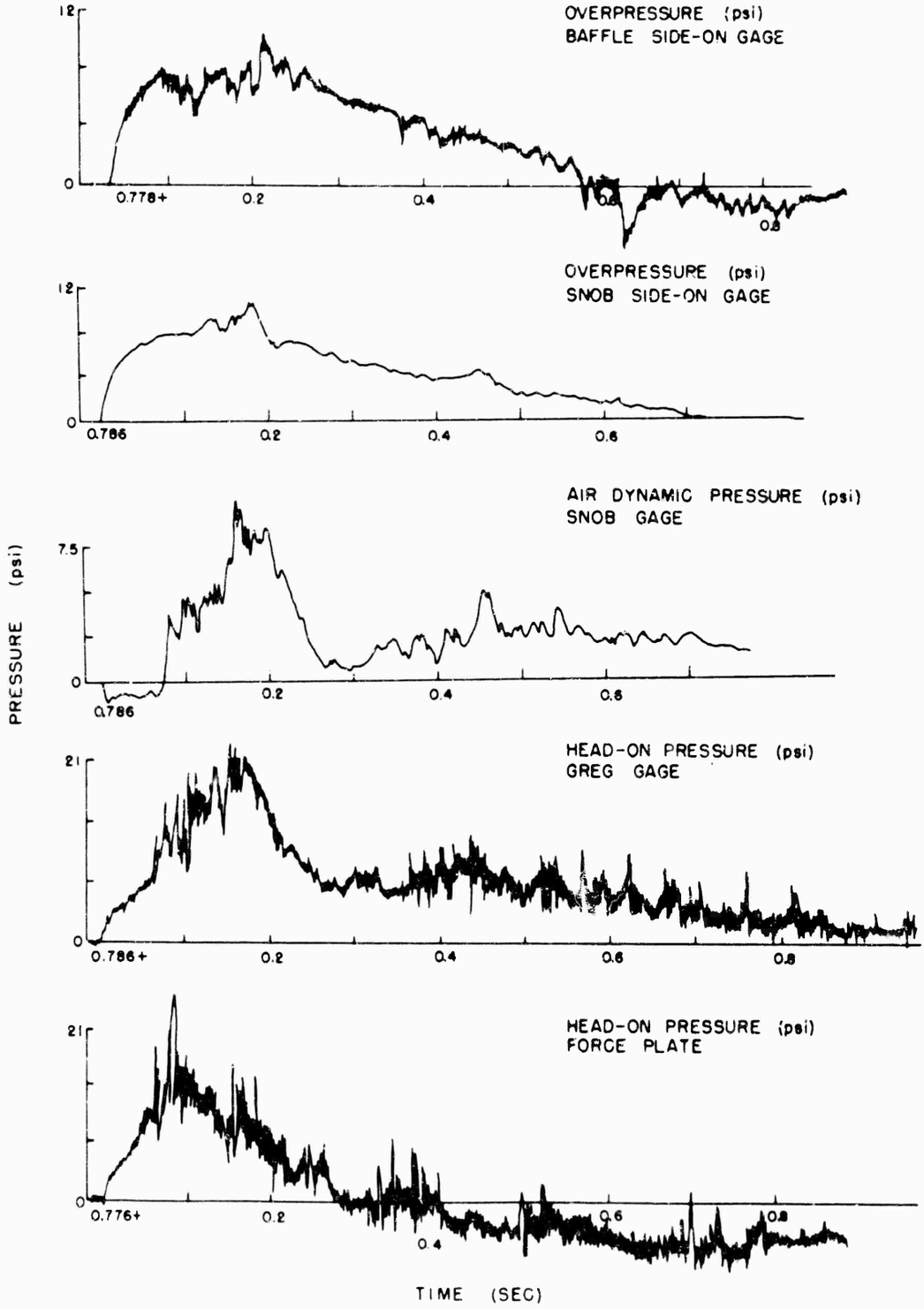

Figure 4.10 Time records of gages at 2,500 ft on desert line (all gage elevations 3 ft, time scale starts on signal arrival).

together with force plate records in Figures 4.15 through 4.19. The derived curve and the force-plate records should agree if the dust behaved exactly as air, otherwise the force plate should, according to theory, exceed the derived.

---

[1] Obviously neither of these is dust in the sense that it is meant over the desert line. "Dust" must be understood to mean any solid or liquid carried in particle form by the air.

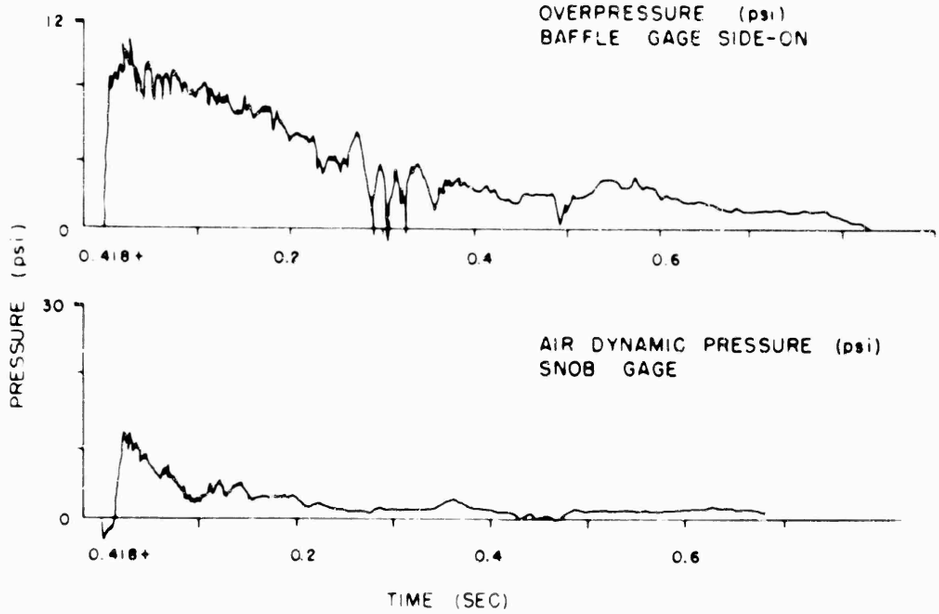

Figure 4.11 Time records of gages at 2,000 ft on the asphalt line (all gage elevations 3 ft, time scale starts on signal arrival).

Comparison is confused by the tendency of the force plate to show a short positive phase. However, the correlation is satisfactory in the early stages, except at 2,500 feet on the desert line where, although the peak values are similar, the peak comes earlier on the force-plate record. As it happened, the instrument tower carrying greg and snob and the one carrying the force plate were 48 feet apart. The difference in wave shape probably represents a real difference of the phenomenon with sampling location and offers a hint about the dangers of overgeneralizing a point measurement.

On the whole, however, the comparison is satisfactory in the initial part of the blast wave and demonstrates that the contribution of dust to head-on stagnation pressure is similar to that of air when the obstacle size is large.

4.3.3 Centripetal Density (Air Density). Transducers at 2,500 feet on the desert line and at 2,000 feet on the asphalt line were destroyed by the zero transient, and the transducer at 2,500 feet on the water line

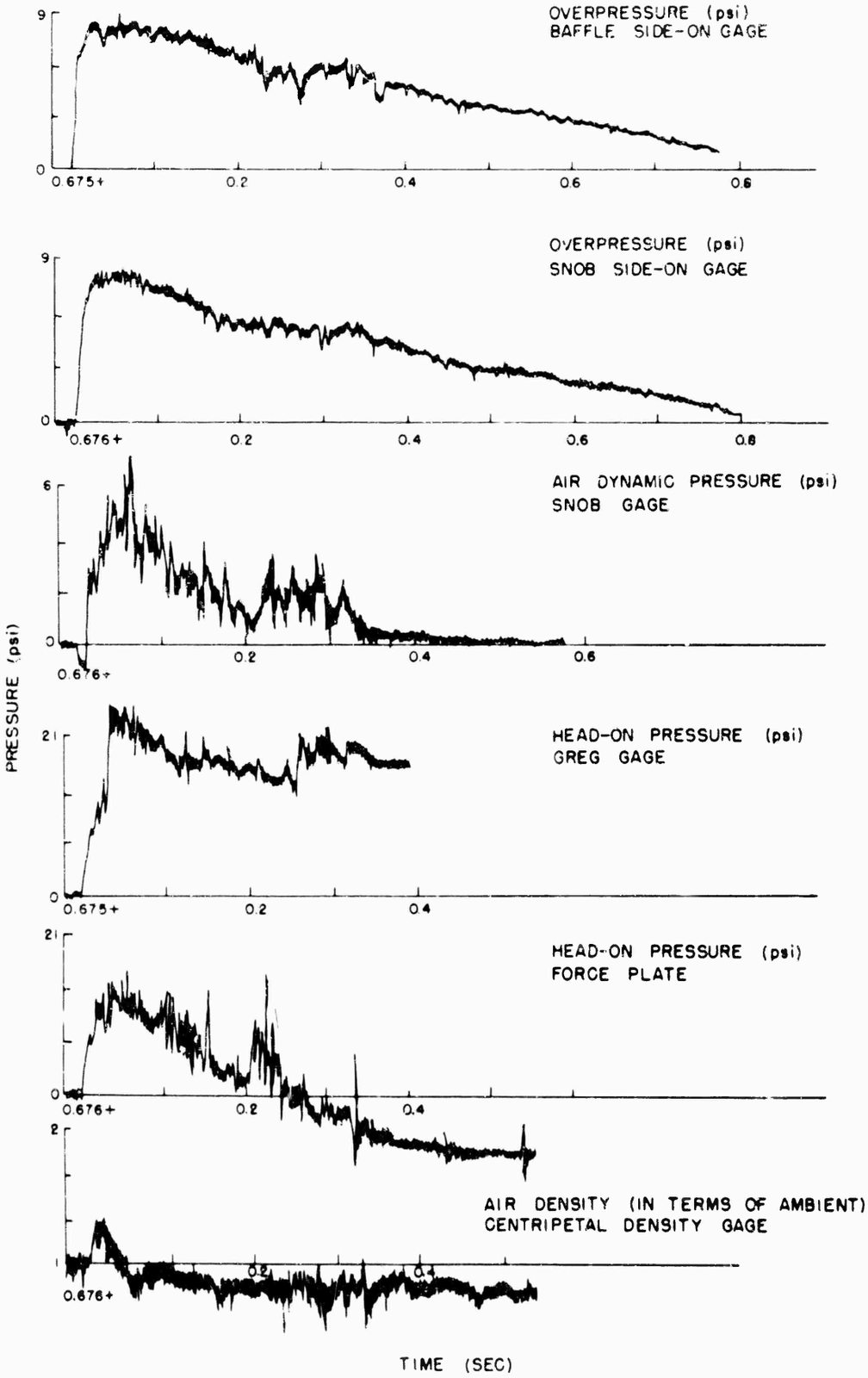

Figure 4.12 Time records of gages at 2,500 ft on asphalt line (all gage elevations 3 ft, time scale starts on signal arrival).

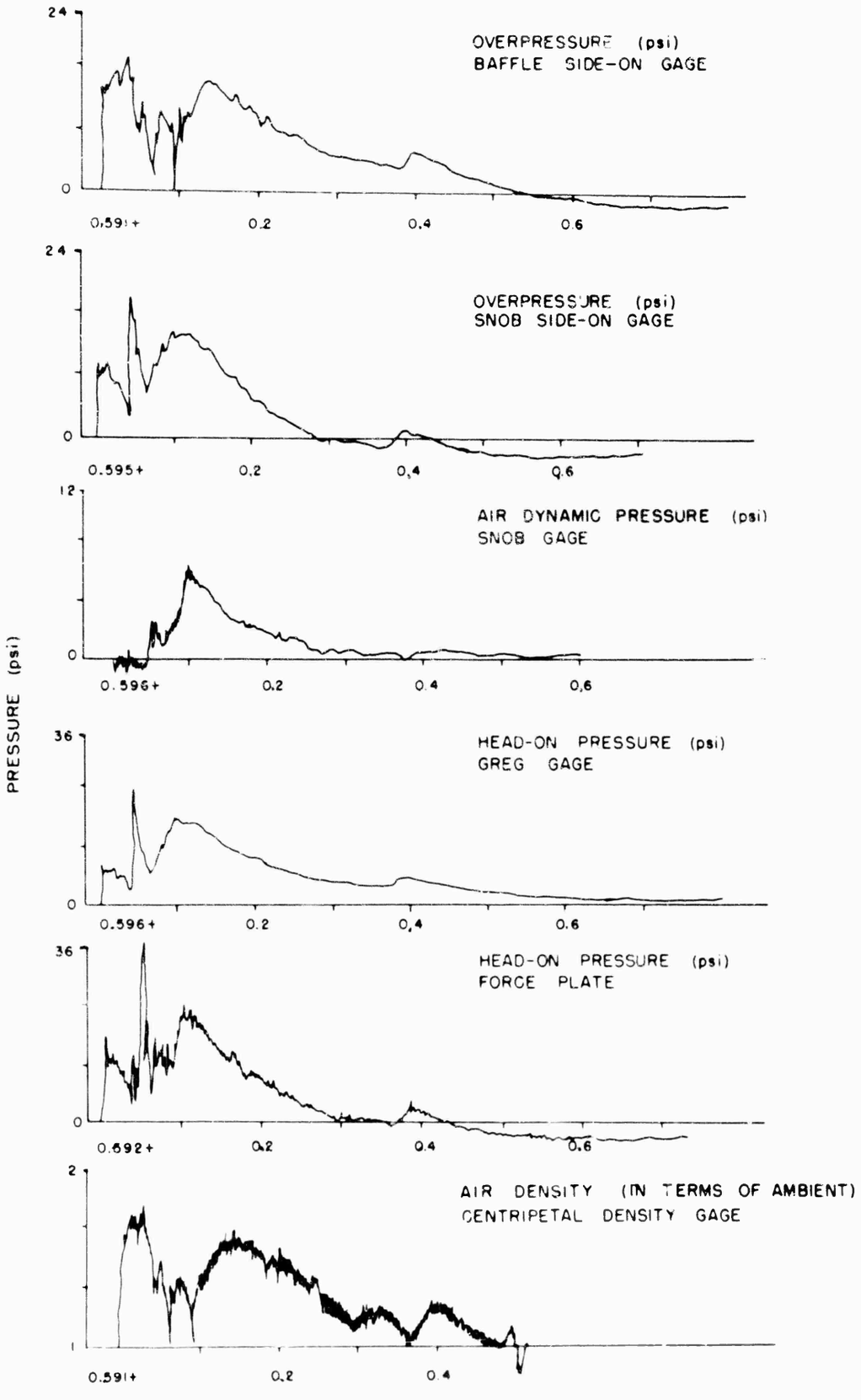

Figure 4.13 Time records of gages at 2,000 ft on the water line (all gage elevations 3 ft, time scale starts on signal arrival).

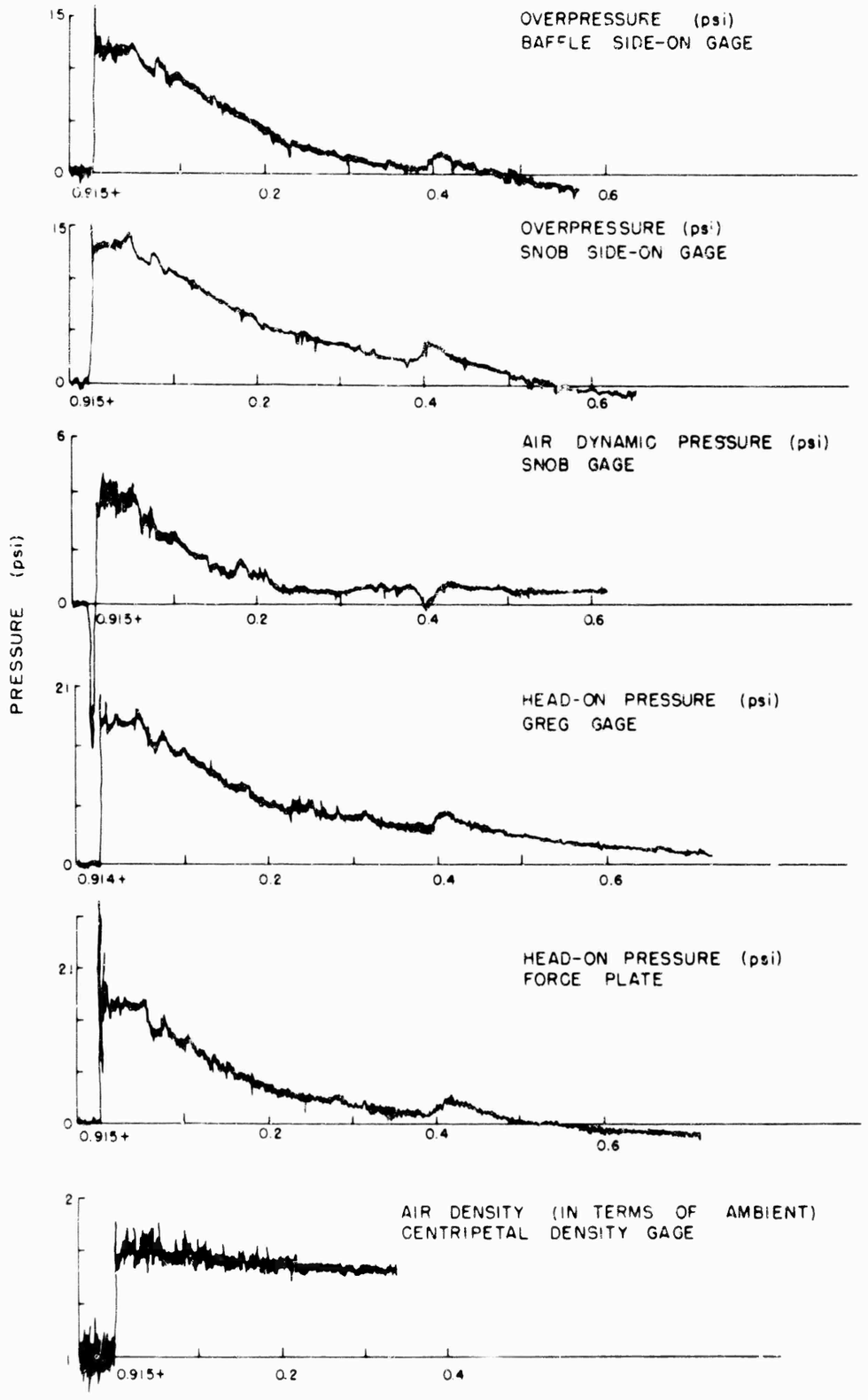

Figure 4.14 Time records of gages at 2,500 ft on water line (all gage elevations 3 ft, time scale starts on signal arrival).

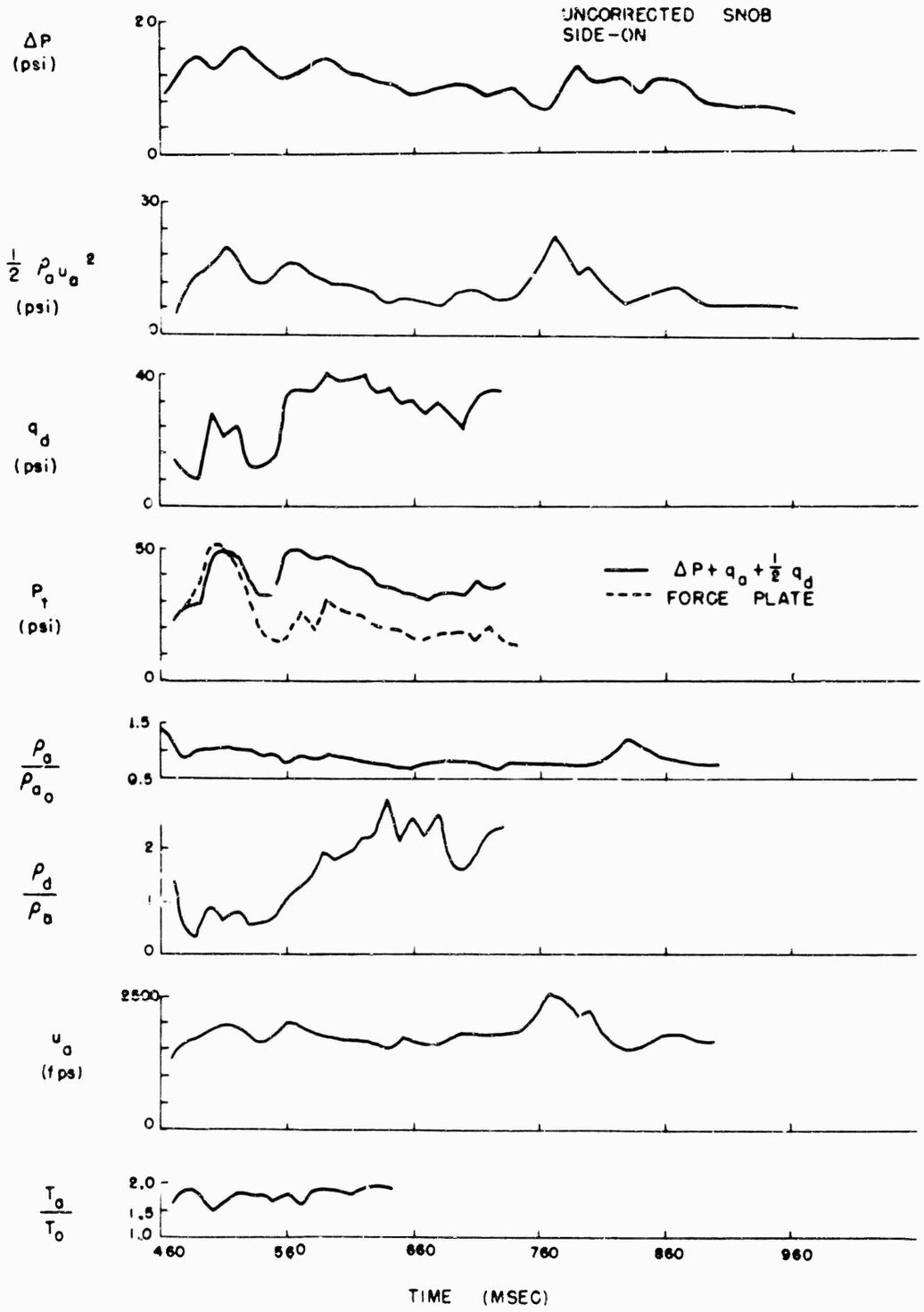

Figure 4.15 Various measured and derived parameter-time records for 2,000 ft (desert).

took a permanent set shortly after the maximum from being plugged with mud. Otherwise, records were satisfactory. Peak values are listed in Table 4.6, and curves for air-density-versus-time are shown in Figures 4.9 through 4.14.

Centripetal-density-gage results were possibly the most unexpected of all the measurements. Air-density-versus-time records on the water line were understandable and satisfied the Rankine-Hugoniot relation after the

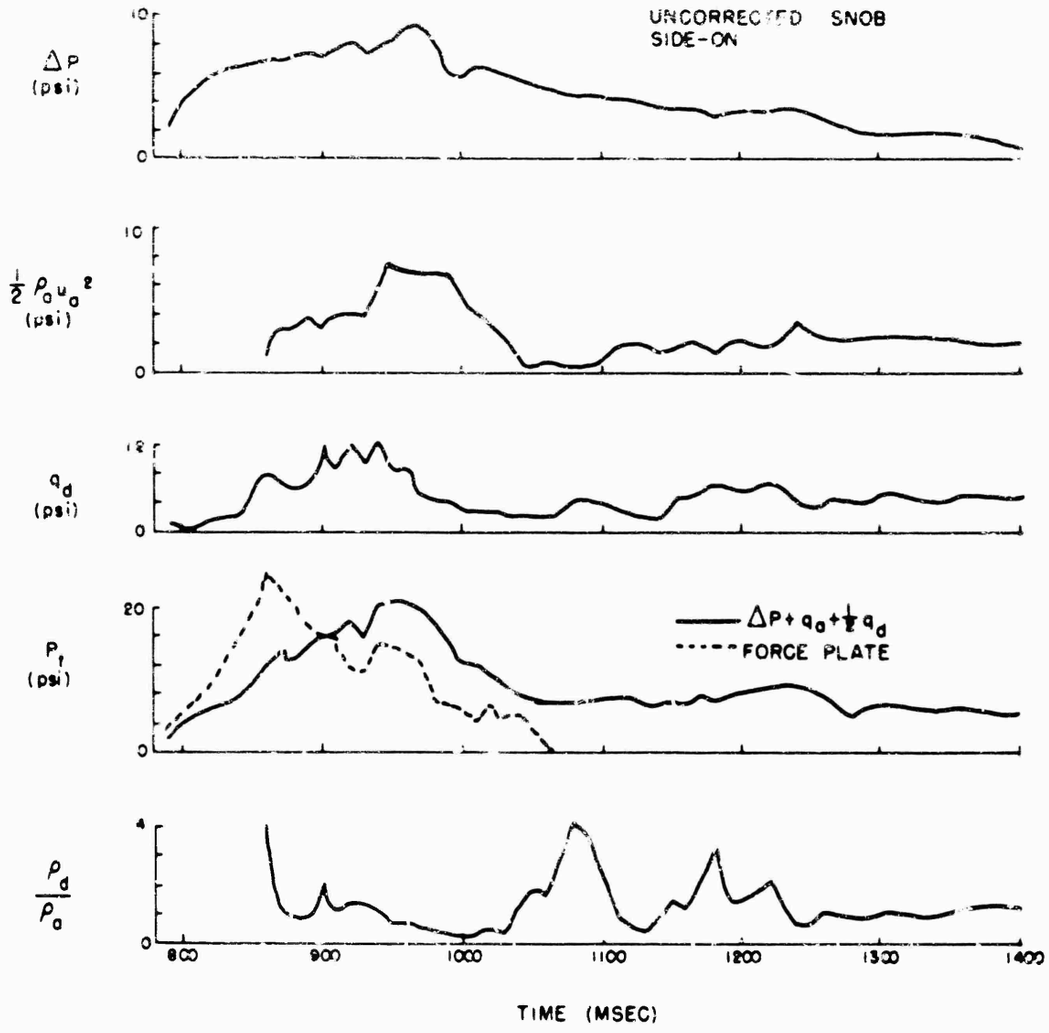

Figure 4.16 Various measured and derived parameter-time records for 2,500 ft (desert).

unusual nature of the overpressure-time curves was taken into account. But on the desert and asphalt lines, air density after an initial increase fell below ambient during most of the blast-wave passage. This phenomenon is probably not as marked as it seems from the record, since the air density prior to shock arrival was lower than the instrument indicated. Apparently preshock air taken into the gage was cooled by gage parts. Even so, the decrease of density with increasing overpressure is startling and probably results from the envelopment of the gage by the hotter air carried along

by the precursor. The result is significant, since it means that high air dynamic pressures are caused not by abnormally high densities but by high velocities.

4.3.4 Particle Velocity. The electronic components of the gage proved too delicate to withstand the zero transient and no usable records were obtained. Since the weakness was encountered prior to Shot 12, only

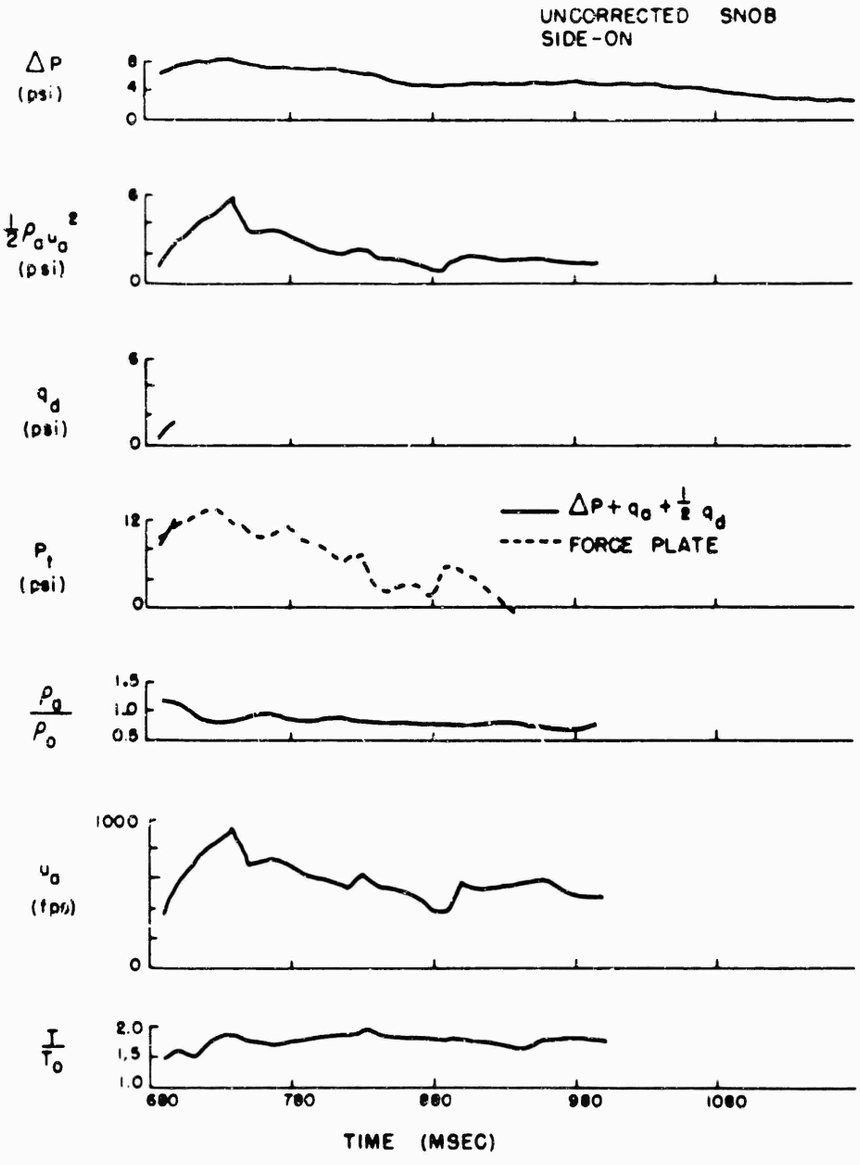

Figure 4.17 Various measured and derived parameter-time records for 2,500 ft (asphalt).

one gage, located at 2,500 feet on the desert line, was activated for that shot. Its output changed at zero time, and was unintelligible after shock arrival.

4.3.5 Medium Density. These instruments, which were intended to determine dust and air density, failed before shock arrival but after zero

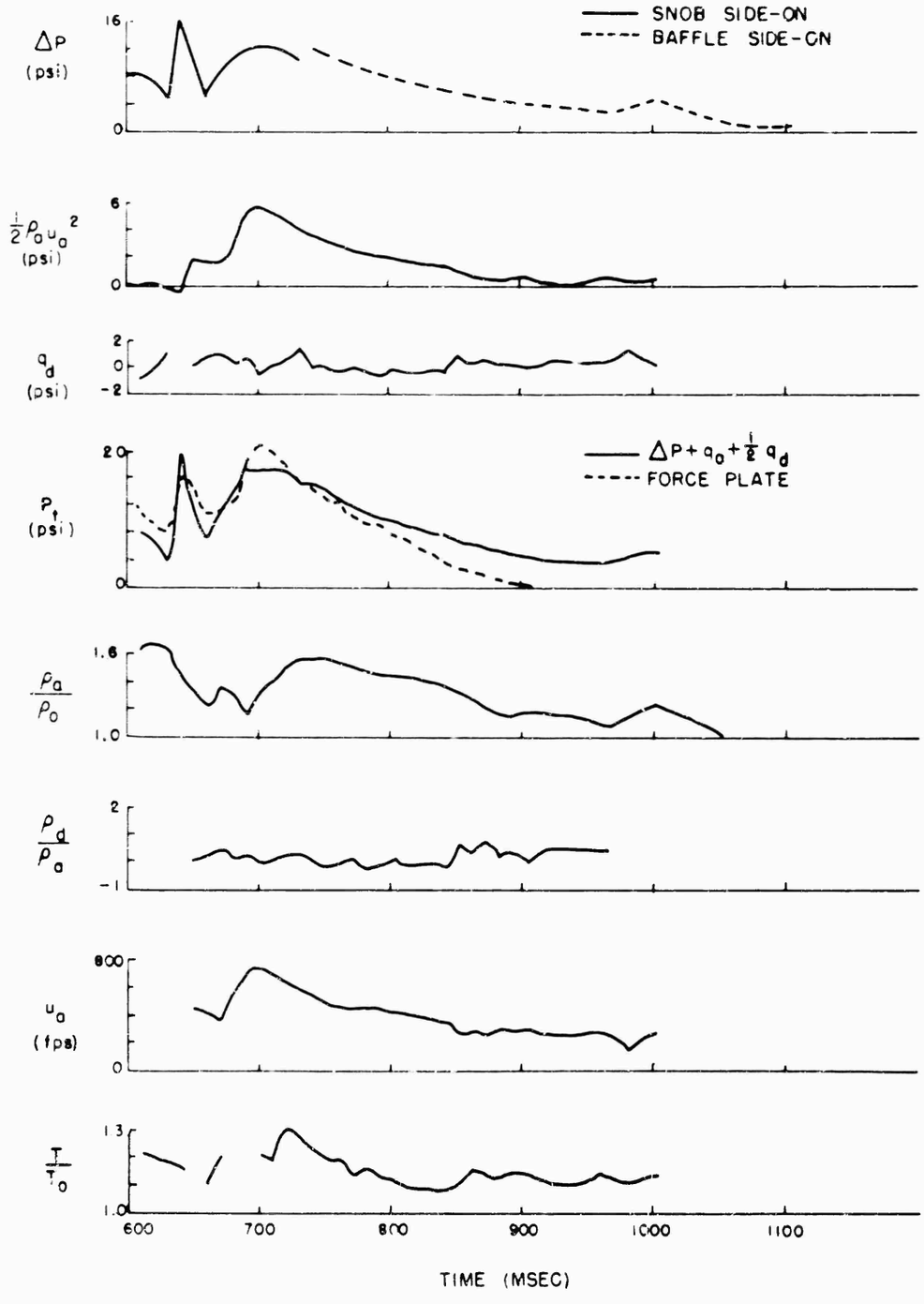

Figure 4.18 Various measured and derived parameter-time records for 2,000 ft (water).

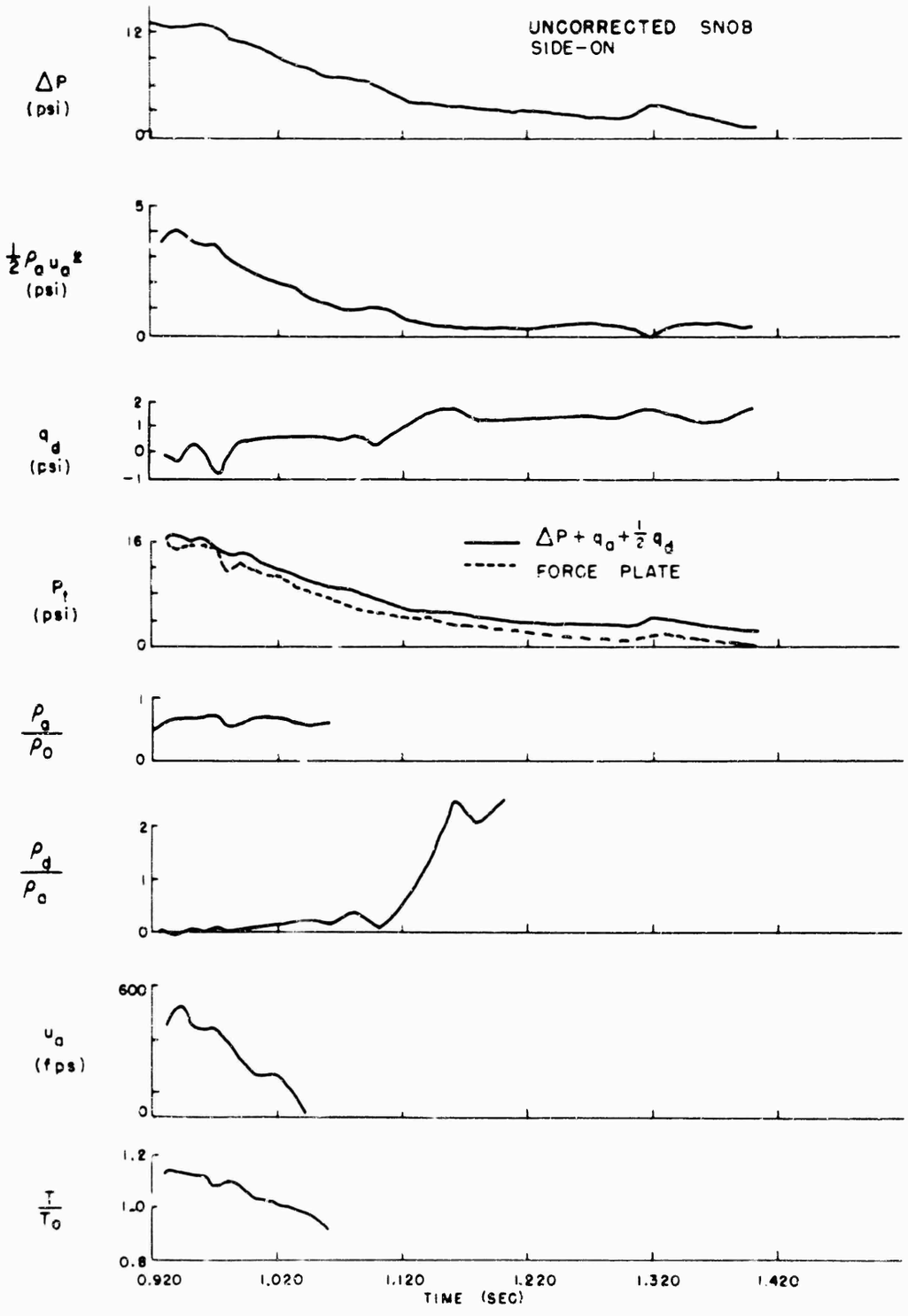

Figure 4.19 Various measured and derived parameter-time records for 2,500 ft (water).

time. Postshot tests indicate that the gage is sensitive to thermal effects.

4.3.6 Overpressure. Overpressures were measured at 2,000 and 2,500 feet on the three lines by two methods. A pressure transducer was situated in the baffle of the centripetal-density gage and a second transducer measured overpressure in the snob gage. Peak values and other data are given in Table 4.7. The snob peak values are corrected by subtracting 4 percent of the uncorrected air dynamic pressure (snob differential). This correction was included to allow for the flow perturbation introduced by the tower and supporting arm of the instrument. Uncorrected overpressure-time records are given in Figures 4.9 through 4.14.

Project 1.11 was not designed to study overpressure per se, but a few records were needed for comparison with other data. Wave shapes over the desert were of the typical precursor type and resemble those obtained on the Upshot-Knothole Shot 1. Over asphalt, overpressures were lower and the wave shapes smoother than those obtained on the desert, but they showed the typical precursor behavior of a slow rise to the maximum overpressure.

On the water line at 2,500 feet, the overpressure exceeded that of the corresponding desert station. The wave shape was nearly classical, except for a slight plateau after shock arrival. Yet, the record obtained at 2,000 feet on the water showed somewhat smaller peak overpressure than did the corresponding desert station. It is thought that the first signal arrived with considerable yaw. All in all, the overpressure-time records obtained at this station are some of the most peculiar obtained in the history of this classical measurement.

A record of pitot-static side-on pressure versus time, obtained at 8,000 feet on the desert line, displayed no serious anomalous behavior. A slight secondary shock was observed on it about 0.52 second after the primary shock arrival.

4.3.7 Derived Quantities and Cross Checks. As suggested before, it is possible to derive various quantities using formulae listed in Table 2.1. These include the ratio of suspended dust to air density, ρ_d/ρ_a, air velocity, u_a, and air temperature, T. Curves of the ratio of dust to air density and the ratio of air temperature to ambient as functions of time are plotted for the various stations in Figures 4.15 through 4.19. For comparison, we have also plotted overpressure (snob side-on) and the ratio of air density to ambient. Also in these figures are dust dynamic pressure, corrected air dynamic pressure, and the calculated head-on pressure for a large obstacle compared with the force-plate results. All time curves are based on average values read at 10-msec intervals. Table 4.8 gives ambient conditions for Shot 12 used for the actual temperature and density computations.

These calculated air velocities are extremely high over the desert and asphalt. The velocities are so high that, at 2,000 feet on the desert line, the flow is briefly above Mach one. From the Rankine Hugoniot relation one would not expect this to occur until the shock strength exceeds 4.8.

Since at 2,500 feet on the water line air dynamic pressure and air density initially satisfy the Rankine Hugoniot relation, so does the air velocity. At the 2,000-foot station this derived air velocity is higher

TABLE 4.5 FORCE PLATE RESULTS (P_t), SHOT 12
(All Gage Elevations 3 ft)

Ground Distance	Surface	Time of Arrival	Maximum		Remarks
			Value	Time	
ft		sec	psi	sec	
2000	Desert	0.452	52	0.493	
	Asphalt				No deflection, gage impaired by zero transient
	Water	0.592	12.0 21.0	0.598 0.691	Narrow spike to 23 psi at 0.640 sec, shows short positive phase
2500	Desert	0.776	24.5	0.858	Shows short positive phase
	Asphalt	0.676	13.5	0.715	Shows short positive phase
	Water	0.915	16.0	0.915	

TABLE 4.6 CENTRIPETAL DENSITY GAGE RESULTS (ρ_a), SHOT 12
(All Gage Elevations 3 ft)

Ground Distance	Surface	Time of Arrival	Maximum		Remarks
			Value	Time	
ft		sec	ρ/ρ_o	sec	
2000	Desert	0.452	1.33	0.456	Density below ambient during much of blast wave passage, shows second spike at 0.824 sec
	Asphalt				Gage out at zero
	Water	0.591	1.68 1.57	0.603 0.733	
2500	Desert				Out at zero
	Asphalt	0.676	1.20	0.685	Density below ambient during most of blast wave passage
	Water	0.915	1.68	0.934	Transducer clogged, as it does not return to ambient density

TABLE 4.7 OVERPRESSURE MEASUREMENTS (ΔP), SHOT 12
(All Gage Elevations 3 ft, Except at 8,000 ft Where 10 ft)

Ground Distance	Surface	Gage Type	Time of Arrival	Maximum		Positive Duration	Remarks
				Value	Time		
ft			sec	ps	sec	sec	
2000	Desert	Baffle	0.452	14.0	0.494 0.521		Gage failed during shock wave passage
		Snob side-on	0.451	15.6	0.518	0.788	
	Asphalt	Baffle	0.418	8.5	0.440	0.820	
		Snob side-on					Gage out at zero
	Water	Baffle	0.591	13.7 12.8	0.604 0.716	0.560	
		Snob side-on	0.595	8.5 12.2	0.610 0.704	0.275	Shows narrow spike at 0.640 sec, short positive phase
2500	Desert	Baffle	0.778	9.2	0.964	0.606	
		Snob side-on	0.786	9.5	0.963	0.700	
	Asphalt	Baffle	0.675	8.0	0.748	0.903	
		Snob side-on	0.676	7.9	0.730	0.874	
	Water	Baffle	0.915	12.6	0.915	0.572	
		Snob side-on	0.915	13.0	0.915 0.958	0.550	
8000	Desert	Pitot static tube side-on	5.304	1.59	5.304	1.276	

than indicated by the Rankine Hugoniot relation.

It was unfortunate that direct measurement of air velocity was not obtained, since this parameter with its abnormally high value seems to account for the high air dynamic pressures observed. However, the indirect results should be accurate to about 10 percent.

TABLE 4.8 AMBIENT CONDITIONS FOR SHOT 12 SURFACE

Ambient Air Temperature	19.5°C
Ambient Sound Speed	1,226 fps
Air Pressure	13.18 psi
Ambient Air Density	1.083×10^{-3} gm/cm^3

The curves for the ratio of suspended dust to air density versus time, which have been computed by assuming air and dust have the same velocity, follow the dust dynamic-pressure curves closely. Dust density shows a tendency to increase as the blast wave passes. The estimate of this ratio becomes increasingly unreliable as the air dynamic pressure decreases.

TABLE 4.9 SHOT 4 RESULTS

Instrument and Quantity Measured	Ground Distance	Elevation	Time of Arrival	Maximum		Remarks
				Value	Time	
	ft	ft	sec		sec	
Wind direction gage, pitch	1350	3	0.249	+9°	0.251	Shows turbulent pitch centered about -2° after initial phase
Wind direction gage, pitch	1850	6	0.405	+29°	0.411	Returns to zero flow at 0.430 sec
Wind direction gage, yaw	2150	4	0.552	+10° -21°	0.730 1.160	Shows initial -15° yaw which then stabilizes to -5° yaw before going to first max, shows a gradual shift between maximum
Snob differential pressure, air dynamic pressure	2150	3	0.532	>15 psi	0.620	Shows upward drift after blast wave passage
Force plate, head-on pressure	2150	3	0.539	>60 psi	0.610	Shows drift prior to shock arrival caused by radiant heating
Snob side-on, overpressure	2150	3	0.532	>20 psi	0.642	Positive phase duration is 0.460 sec

These estimates of suspended dust densities exceed preliminary results obtained by Project 1.13 at both the 2,000- and 2,500-foot stations on the desert line (Reference 15).

Curves for air temperature versus time are included for completeness, although they essentially reflect the behavior of air-density measurements

on the desert and asphalt lines. These curves were useful with air velocity for computing Mach-flow corrections.

4.3.8 Comments on Errors. Pitch measurements are probably accurate to ± 1 degree or 5 percent of the deflection, whichever is greater.

By examining consistency of successive calibrations, one finds that the error of the peak values for pressure should be less than 5 percent. For values other than the peak, the error may be estimated as 5 percent of the value or 2 percent of the peak, whichever is greater. If the instrument is injured the deflection is of little or no physical significance. Gages showing abnormal positive-phase durations are valid only for a brief interval after shock arrival.

Errors of derived quantities must be individually estimated by considering possible errors of the source quantities and error amplification in computation. Since dust dynamic pressure and ratio of dust to air density are based on differences of measured quantities, errors may be considerable, particularly on the water line (where differences are small).

4.3.9 Shot 4 Results. Shot 4 (Turk) was detonated at 0520 PST on March 7, 1955, on a 500-foot tower located in Area 2 of Yucca Flat. The yield was 43 kt. A number of records were obtained. Since set ranges were low, it is not feasible to specify peak values for some of these records; instead, a lower limit is given. Results are listed in Table 4.9.

Chapter 5
CONCLUSIONS AND RECOMMENDATIONS

5.1 CONCLUSIONS

5.1.1 Wind Direction Measurements.

1. Considerable pitch was found on all lines, even on the water line where none was expected.

2. On the desert and asphalt lines, pitch was initially upward and then horizontal or downward, the downward flow being strongest at 2,500 feet. In general, initial pitch decreased with distance (except at the beginning of the desert line) and the duration of upward flow increased with distance. Initial pitches were greater over the asphalt line than the desert line.

3. Pitch predicted from photographic and time-of-arrival data agrees with initial pitch at the 10-foot asphalt stations but is greater than that measured over the desert line. Initial pitch at 3-foot stations was much smaller than at 10-foot stations.

4. Downward flow at 2,500-foot stations on both lines began at the same time, one second after burst, and shortly after the expected arrival time of the main shock.

5. Pitch records over water were much more erratic than over desert or asphalt and suggest large-scale turbulence.

6. No significant systematic yaw was observed where the instruments functioned.

5.1.2 Other Measurements.

1. Air dynamic pressures at 3-foot elevations were highest over desert, next high over asphalt, and least high over water.

2. At 3 feet over desert, dust pressures were larger than air dynamic pressures; over asphalt some dust pressure was present but the amount is uncertain, over water it was effectively zero. Desert line dust contributed about half of the product of its density and the square of its velocity to stagnation pressure exerted on the sizeable force plate.

3. On asphalt and desert lines, air dynamic pressures were much higher than would be inferred from the measured overpressure using Rankine Hugoniot relations. This was also true on the 2,000-foot water station, but at the 2,500-foot water station agreement was achieved.

4. Densities on the water line followed the pressure and initially satisfied the Rankine Hugoniot relations. On the desert and asphalt lines, densities were low, below ambient during most of the blast.

5. Overpressures recorded at the 2,000-foot water station were not ideal; two shocks and a slower pressure rise are evident. Times of ar-

rival and gage response suggest that the first shock arrived with considerable yaw.

6. At 8,000 feet over desert, dynamic pressure and overpressure were ideal and in the correct Rankine Hugoniot relation.

5.1.3 General Conclusions. Initial flow behavior on desert and asphalt seems to have been much as would be expected. The flow was at first upward and later more nearly horizontal; near the surface, the flow was nearly horizontal at all times. The results over water were unpredicted and correspond to the unusual nature of the blast wave over that area.

The appeal to the Bernoulli principle is not substantiated, since the sum of overpressure and air dynamic pressure was not constant at the same ground distances on the three surfaces; if one adds the dust dynamic pressure, the difference is even more pronounced.

The contribution of dust to dynamic pressures is well established, since the dust dynamic pressure exceeded that of air on the desert line. Even disregarding the dust, air dynamic pressures were still much higher than would be expected from measured overpressure and Rankine Hugoniot relations. In fact, air dynamic pressures over the desert exceed ideal by a factor of more than one half, while they were comparable to or less than ideal at stations over asphalt and water.[1] Density measurements show these excessive air dynamic pressures over the desert were caused by high air velocity, not increased air densities. Since the fine dust of Frenchman Flat should accelerate to air speed in a few milliseconds the dust also had a high velocity.

Force-plate results suggest that Frenchman Flat dust behaves much as air in its flow about it, i.e., the registering coefficient of dust for the force plate is about one half.

We have examined corrections to dynamic pressure for the psuedo-spherical nature of the shock configuration (Appendix C). This correction is too small (except on the water line at 2,000 feet) to account for high air dynamic pressures, unless one assumes a spherical expansion from a source much nearer the gage station than ground zero.

At this point it is realized that this resembles the arguments of Hess because this nearer source implies an internal flow structure (Reference 4). Pitch-time records fail to show the presence of a flow such as Hess predicted, except possibly at the 2,500-foot stations over asphalt and desert; the upward, then downward, flow noticed there is the pattern that would be expected from vortex passage. On the other hand, the simultaneous downward flow at 2,500 feet on both desert and asphalt, which came shortly after shock arrival on the water line, could represent a feed-through of energy from the shocked air above the precursor. Such a flow would supply the required expansion from a point closer than ground zero.

The weakness of this hypothesis is that downward flow was not observed at the closer stations, although it may be that the feed-through there was more nearly horizontal or took place above the 10-foot gage position.

In summary, we propose tentatively that high dynamic pressures are the result of high air velocities brought about by some feed-through from the energy source of the sphere of shocked air above the precursor. We

[1] Ideal air dynamic pressures are described in ITR-1153 (Reference 2).

can say little about this flow pattern beyond that the results at 2,500 feet on the desert and asphalt suggest that it exists. Whether it is the pattern proposed by Hess is open to question.

Certainly, more work is required, theoretical and experimental, before the precursor phenomenon will be completely understood.

5.2 RECOMMENDATIONS

Project 1.11 accomplished its objectives: the examination of precursor afterflow direction and the nature of dynamic pressure. At the same time, the experiment revealed tantalizing academic questions. Perhaps the answers to these questions will aid in the understanding of the precursor phenomenon and will allow prediction of its effects over surfaces other than those instrumented on Shot 12.

Should another precursor-study shot be planned, it is recommended that: (1) a test be conducted over a surface where sand rather than silt is present, since such soil typifies deserts where the precursor might be used tactically; (2) the test be made with a device of different yield than that of Shot 12 to examine scaling laws; (3) pitch-time measurements be made at higher elevations at the closer stations than were made on Shot 12 to further reveal precursor afterflow pattern; (4) more extensive yaw-time measurements be taken; and (5) the instruments which were successful in Shot 12 be used at two elevations to examine the variation with height of dynamic pressure parameters.

It is also recommended that additional data be obtained on the dust loading of obstacles. This can be adequately studied on a laboratory scale with a few field checks. Theoretical studies of precursor afterflow should be continued, now that Shot 12 has provided results to serve as a basis for and as a check on such endeavors.

Appendix A
THEORY OF THE SNOB AND GREG DUST RESPONSE

Operational principles of snob and greg gages may be explained by some elementary examination of the hydrodynamic behavior of a mixture of air and dust. For this analysis, we may assume that the mass of suspended dust and the mass of the air in which the dust is suspended are comparable. This leads to two interesting conclusions: (1) The volume occupied by the dust is entirely insignificant, which means that the air has the usual equation of state. (2) The suspended dust exerts no appreciable static pressure because the air molecules greatly outnumber dust particles. With these considerations in mind, the hydrodynamic equations concerned with conservation of mass and momentum may be written as follows:

Conservation of mass:

$$\frac{-\partial \rho_a}{\partial t} = \nabla \cdot (\rho_a \vec{u}_a) \qquad (A.1)$$

$$\frac{-\partial \rho_d}{\partial t} = \nabla \cdot (\rho_d \vec{u}_d) \qquad (A.2)$$

Conservation of momentum:

$$-\nabla P = \rho_a \frac{d\vec{u}_a}{dt} + \rho_d \frac{d\vec{u}_d}{dt} \qquad (A.3)$$

Here ρ indicates densities, P is pressure, $\vec{u}$ is vector velocity, and t is time. The subscripts a and d refer respectively to air and dust; standard vector notation is used. The mass conservation equations are entirely obvious; the momentum conservation equation may be derived most easily by regarding the time rate at which momentum is given to dust as a force on the air of opposite direction.

These equations may be specialized by taking a steady-flow case expressed in cylindrical coordinates, where that flow is symmetric with respect to azimuth angle. These equations then are:

$$0 = \frac{\partial}{\partial r} (\rho_a u_{ar}) + \frac{\partial}{\partial z} (\rho_a u_{az}) \qquad (A.4)$$

$$0 = \frac{\partial}{\partial r} (\rho_d u_{dr}) + \frac{\partial}{\partial z} (\rho_d u_{dz}) \qquad (A.5)$$

$$-\frac{\partial P}{\partial z} = \rho_a \frac{\partial}{\partial r}(u_{az}) + \rho_d \frac{d}{dt}(u_{dz}) \qquad (A.6)$$

$$-\frac{\partial P}{\partial r} = \rho_a \frac{\partial}{\partial r}(u_{ar}) + \rho_d \frac{d}{dt}(u_{dr}) \qquad (A.7)$$

Here r is radial and z is the polar coordinate; the coordinates which are used as subscripts refer to the component of the velocity in that direction. If it now is assumed that the flow is incompressible, a rather surprising result is obtained. Since the mass conservation equation is unchanged by the pressure of dust, the same form for the flow potential is implied. This means that the steady-state flow of an incompressible fluid is the same whether dust is present or not and in spite of friction. This is true because the presence of dust does not alter the boundary condition and only one solution exists for the potential function.

Since air actually is compressible, considerable alteration of flow because of the dust can be expected. But at least the dust behavior can be approximated by assuming that the air flow is unchanged by the presence of dust. Even with this simplification, the problem is not an easy one; the actual computation of particle trajectories usually must be done using machine methods (Reference 16). For calculating dust response of snob and greg, the head-pressure enhancement caused by dust may be computed, considering dust traveling along the axis of symmetry. Equation A.6 is used for this computation by breaking the pressure changes from free stream into two parts: namely, ΔP_d caused by dust momentum changes, and ΔP_a caused by air momentum changes.

From the incompressible flow results discussed above, the air momentum changes give a contribution to stagnation pressure unaffected by the presence of dust. On the axis of symmetry the dust contribution to pressure amounts to:

$$\Delta P_d = -(\rho_d u_{dz})_o \Delta u_{dz} \qquad (A.8)$$

In this expression, $(\rho_d u_{dz})_o$ is the dust mass flux in the free stream, and Δu_{dz} is the change of velocity suffered by dust because of the flow about the obstacle. This expression is derived by a combined use of the momentum and mass-conservation equations in an integration which neglects the small radial divergence terms. In the snob gage, the small response to dust is achieved by reducing the term Δu_{dz} by means discussed in a section on that instrument. The response of the gage may be calculated by assuming that dust particles behave as spheres with the same diameters as the dust particles under consideration. Then, knowing the flow conditions, dust density, etc., Δu_{dz} may be calculated. The latter quantity varies strongly with particle diameter and to lesser extent with flow velocity. The ratio of Δu_{dz} to $(u_{dz})_o$ is negligibly small for particle diameters in excess of ten microns.

The same expression (Equation A.8) may also be used to calculate the greg response, provided the particles are completely slowed before they strike the diaphragm. For larger particles, however, this will not be the case; their stopping distance is such that they strike the diaphragm and

rebound. Dust particles nevertheless will still register a dynamic pressure of $(\rho_d u_d^2)_o$ if the mean free path of the rebounding particle is small compared to gage dimensions. This occurs because the momentum of the oncoming particle is reduced by that of rebounding particles. The dust density is made high enough to satisfy this condition by having the gage opening act as a dust trap.

In the preceding argument, it was assumed that flow was head-on and that the particles were not appreciably deviated by the air flow about the gage. Particles with a diameter of less than 10 microns are appreciably deviated and show a transitional behavior registering between the $(\rho_d u_{dz}^2)_o$ of the larger particles and the $1/2\ (\rho_d u_{dz}^2)_o$ that would be expected if the dust behaved exactly the same as air.

Appendix B

THEORETICAL TREATMENT OF THE MEDIUM-DENSITY-CAPACITY GAGE

The most detailed analysis of the response of this gage to suspended dust is accomplished by regarding suspended dust particles as a set of small spheres distributed throughout the air. To simplify the analysis further, the electric field is regarded as uniform rather than radial; this assumption makes it possible to calculate the polarization of the spheres which represented dust particles. Furthermore, both the small terms involving the interactions of the spheres and the small effect of changes in air density are ignored. Thus the medium is regarded as a mixture of ordinary air and rarefied dust gas which have dipole moments proportional to the electric field impressed on the particles. Using this approach, it was found that the suspended dust contribution to medium dielectric constant (ΔK_d) may be expressed as follows:[1]

$$\Delta K_d = \frac{3\rho_d}{\delta} \frac{k_d - 1}{k_d + 2} \qquad \text{(B.1)}$$

Here ρ_d is the suspended dust mass density, δ is the dust bulk density, and k_d is the bulk dielectric constant of the dust. This contribution was independent of the size of the dust particles.

Contributions of a change of air density to a variation of the medium dielectric is easily calculable because the variation (ΔK_a) is directly proportional to the change of air density. Specifically, the relation is:

$$\Delta K_a = 0.447\ \rho_a \qquad \text{(B.2)}$$

Here ρ_a is the air density change in grams per cubic centimeters.

Having examined the contributions of suspended dust and of air density changes, the effect of these changes on both the capacity of the detector and the output frequency is considered next. With no air or dust present, the output frequency (ν_o) is:

$$\nu_o = \frac{1}{2\pi} \frac{1}{\sqrt{L\ C_o}} \qquad \text{(B.3)}$$

Here L is the inductance of the variable tank circuit, and C_o is the capacitance of the exposed capacitor in a vacuum. The value of capacitance is proportional to the dielectric constant of the medium. Accordingly in

---

[1] This problem was solved by J. W. S. Rayleigh in 1892 (Reference 17).

the test conditions this capacitance had a value described by the following relation:

$$C = C_o \left[1 + 0.447\ \rho_a + \frac{3\rho_d}{\delta} \left(\frac{k_d - 1}{k_d + 2} \right) \right] \qquad (B.4)$$

The symbols used in the above equation were defined earlier in the appendix. Using an expression analogous to Equation B.3, and substituting Equation B.4, the frequency in the presence of air and dust is computed. This frequency (ν) is found to be:

$$\nu = \nu_o \left[1 + 0.447\ \rho_a + \frac{3\rho_d}{\delta} \left(\frac{k_d - 1}{k_d + 2} \right) \right]^{-1/2} \qquad (B.5)$$

The variations of frequency with suspended dust density or air density changes may be examined. While Equation B.5 may be used directly for this purpose, it was more convenient to use the differentiated forms as follows:

$$\frac{\partial \nu}{\partial \rho_d} \cong - \nu_o \frac{3}{2\delta} \left(\frac{k_d - 1}{k_d + 2} \right) \qquad (B.6)$$

$$\frac{\partial \nu}{\partial \rho_a} \cong - 0.2235\ \nu_o \qquad (B.7)$$

These forms consider the term raised to the minus one-half power in Equation B.6 to be approximately one after differentiation. This is justified because ρ_a and ρ_d are small compared to one. The density of suspended dust then may be readily calculated as shown in Equation B.8 below by using the shift of the beat frequency from its preshock value ($\Delta \nu$) and knowledge of the change in air density ($\Delta \rho_a$):

$$\rho_d \cong \left(\frac{\Delta \nu}{\nu_o} - 0.2735\ \nu_o\ \Delta \rho_a \right) \frac{2\delta}{3} \left(\frac{k_d + 2}{k_d - 1} \right) \qquad (B.8)$$

Appendix C
CORRECTIONS OF DYNAMIC PRESSURE FOR SPHERICAL DIVERGENCE REFERENCES

Whitener has pointed out that dynamic pressures calculated from Rankine Hugoniot relations are correct only at shock front in the spherical case (Reference 6). As an example, Whitener examined IBM Problem M and found that throughout the positive phase, for distances of 400 and 600 feet, actual dynamic pressures exceed considerably those calculated from the Rankine Hugoniot relation.

Whitener also shows for isentropic spherical expansion that dynamic pressures of the wave interior must exceed those calculated with the Rankine Hugoniot relations. The approximate factor (D) of the actual dynamic pressure that exceeds that calculated by the Rankine Hugoniot relation is given by

$$D = \left(1 + \frac{\int_{c-} \frac{2uc}{c_o R}\, dt}{5(\xi^{1/7} - 1)} \right)^2 \qquad (C.1)$$

Here u is mass velocity, c is the local speed of sound, t is time, c_o is ambient speed of sound, R is radius, and ξ is the ratio of pressure to ambient pressure. This expression should be nearly valid for values of ξ up to eight. The integral in the numerator is to be evaluated along the negative characteristic u - c, i.e., dR/dt = u - c. An example of a characteristic for the case c > u and signal arrival is given in the world diagram, Figure C.1.

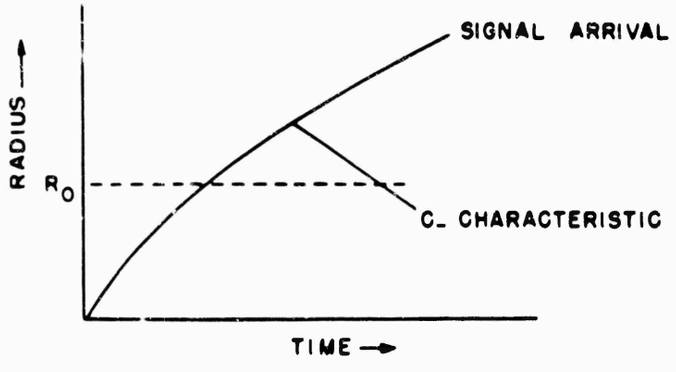

Figure C.1 Sample characteristic and signal arrival---world diagram.

This figure has interesting implications. We may estimate the values of u and c as a function of time from experimental results obtained at a

set of gages situated at, say, R_o. This means we may, in turn, estimate an upper limit for the correction factor D for the case c > u because

$$\int_{R = R_o} \frac{2uc}{c_o R_o}\, dt > \int_{C-} \frac{2uc}{c_o R}\, dt \qquad (C.2)$$

where the first integral is conducted from signal arrival until the time of peak dynamic pressure at $R = R_o$. This is true because u and c diminish with increasing R, the radius along the negative characteristic is greater than R_o, and the integral is carried out for a longer time period along $R = R_o$ than along the characteristic. For u > c the argument could be inverted to establish a lower limit of the value of the integration along the characteristic.

Table C.1 lists these maximum correction factors for various stations. Also given in the table are values of air dynamic pressure calculated from the Rankine Hugoniot relation and overpressure, the product of this quantity

TABLE C.1 SPHERICAL DIVERGENCE CALCULATIONS

Location	Air Dynamic Pressure from Rankine Hugoniot Relation	Maximum Correction Factor D	Product of Rankine Hugoniot Value and D	Observed Air Dynamic Pressure	Maximum Distance to Virtual Source	Horizontal Distance from Precursor Toe to Main Shock
	psi		psi	psi	ft	ft
2,000-ft, Desert	5.2	1.23	6.4	20.0	230	280
2,500-ft, Asphalt	1.63	1.07	1.75	7.8	65	330
2,000-ft, Water	3.58	1.12	4.0	5.8	430	-

and the correction factors, and observed air dynamic pressure which are corrected for Mach effects. The estimation of the correction factor D is approximate on the water line, since air velocity is uncertain for the period the air dynamic pressure showed a negative value. We have chosen to ignore this period in the integration.

On the water line this maximum correction factor approaches accounting for dynamic pressure enhancement above the Rankine Hugoniot value. On desert and asphalt, however, it falls far short of bringing calculated and observed air dynamic pressures into accordance. If one, instead, assumed a cylindrical divergence, the correction factor would be less than for the spherical case.

There is another possibility which would allow flow divergence to account for these high dynamic pressures. This is to regard diverging flow originating not at ground zero but from a point much nearer the gage station. This virtual source may be considered a feed-through from the sphere of shocked air into the precursor. Such maximum radii are also listed on the table for sake of comparison. Their physical significance is highly

questionable, as the precursor does not, of course, exhibit a spherical divergence but, rather, some more complicated geometry not easily amenable to analytical methods. For further comparison we have also listed the separation of the precursor shock front from the sphere of shocked air above the precursor when the precursor strikes the station. These have been estimated by observing the distance the precursor leads the blast wave on the water line.

The divergence correction application now resembles the arguments of Hess; we are now appealing to an internal flow pattern within the precursor (Reference 4).

REFERENCES

1. Bryant, E., and others; Statistical Estimation of Damage to Ordnance Equipment Exposed to Nuclear Blasts; Operation UPSHOT-KNOTHOLE, WT-733, March 12, 1954; SECRET RESTRICTED DATA.

2. Summary Report of the Technical Director; Operation TEAPOT, ITR-1153, June 1955; SECRET RESTRICTED DATA.

3. Moore, G. T.; Effects on Engineer Bridging Equipment; Operation UPSHOT-KNOTHOLE, WT-734, January 4, 1954; CONFIDENTIAL RESTRICTED DATA.

4. Hess, R. V., The Interaction of a Shock Wave with a Thermal Boundary (unpublished), see also Bleakney, W., and Griffith, W. C., Diffusion Analogy to Interaction of a Shock with a Thermal Boundary Layer; Princeton University Department of Physics, PU-TN-11-17, January 3, 1955.

5. Broyles, C. D.; Dynamic Pressure vs Time and Supporting Air Blast Measurements; Operation UPSHOT-KNOTHOLE, WT-714, February 1954; SECRET RESTRICTED DATA.

6. Whitener, J. E.; The Behavior of Pressure in the Precursor Region; AFSWC-TN-55-3, March 10, 1955; SECRET DEFENSE INFORMATION.

7. Banister, J. R., and Gentry, V. L.; Three Proposed Measuring Instruments for Use in Dust-Laden Shock Waves; Sandia Corporation, TM-156-54-51, August 2, 1954; OFFICIAL USE ONLY.

8. Church, P. K.; Sandia Diaphragm-Type Pressure Transducer for Shock Wave Measurements; Sandia Corporation, SC-3305(TR), January 6, 1954.

9. Perret, W. R., and Gentry, V. L.; Free Field Measurements of Earth Stress, Strain, and Ground Motion; Operation UPSHOT-KNOTHOLE, WT-716, February 1955; SECRET RESTRICTED DATA.

10. Church, P. K., and Valentine, J. W.; Density Gage for Air Shock Wave Measurements; Sandia Corporation, SC-3004(TR), October 15, 1953; SPECIFIED DISTRIBUTION ONLY.

11. Broyles, C. D., and Merritt, M. L.; Dynamic Pressure Measurements; Operation CASTLE, WT-906, December 1955; SECRET RESTRICTED DATA.

12. Laursen, H. G.; Wind Velocity Gage, Model II; Sandia Corporation, TM-234-54-52, October 19, 1954; UNCLASSIFIED.

13. Cowan, M., and Sander, H. H.; A Gauge for Dust Density Measurement in Blast Waves; Sandia Corporation, TM-137-54-51, May 1, 1954; UNCLASSIFIED.

14. Rollosson, G. W.; Static and Dynamic Overpressure Measurements; Operation TEAPOT, ITR-1192, May 1955; CONFIDENTIAL RESTRICTED DATA.

15. Gordon, M. G., and Bouton, E. H.; Dust Density vs Time and Distance in the Shock Wave; Operation TEAPOT, ITR-1113, May 1955; CONFIDENTIAL RESTRICTED DATA.

16. Langmuir, I., and Blodgett, K. B.; A Mathematical Investigation of Water Droplet Trajectories; AAF Technical Report, February 19, 1946.

17. Rayleigh, J. W. S.; Philosophic Magazine, Vol. 5, No. 34, 1892, p. 481; UNCLASSIFIED.